EUROPEAN ORGANIZATION FOR NUCLEAR RESEARCH

CERN-PPE/92-173
October 12th, 1992

The DELPHI Microvertex Detector

N.Bingefors, H.Borner, R.Boulter, M.Caccia, V.Chabaud, H.Dijkstra, P.Eerola, E.Gross, R.Horisberger, L.Hubbeling, B.Hyams, M.Karlsson, G.Maehlum, K.Ratz, I.Roditi, J.Straver, W.Trischuk, P.Weilhammer
CERN, CH-1211 Geneva 23, Switzerland

Y.Dufour
College de France, Lab. de Physique Corpusculaire, Paris, France

P.Brückman, P.Jalocha, P.Kapusta, M.Turala, A.Zalewska
Institute of Nuclear Physics, Cracow, Poland

J.Lindgren, R.Orava, K.Österberg, C.Ronnqvist, H.Saarikko, J.P.Saarikko, T.Tuuva
Research Inst. for High Energy Physics, Helsinki, Finland

B.d'Almagne, P.Bambade, F.Couchot, F.Fulda
Laboratoire de l'Accélérateur Lineaire, Orsay, France

A.Amery, P.S.L.Booth, A.R.Campion, R.McNulty, N.A.Smith
Univ. of Liverpool, Dept. of Physics, Liverpool, Great Britain

A.Andreazza, M.Battaglia, P.Biffi, V.Bonvicini, W.Kucewicz, C.Meroni, N.Redaelli, A.Stocchi, C.Troncon, G.Vegni
Univ. di Milano, Dipt. di Fisica, Milano, Italy

P.Dauncey
Univ. of Oxford, Dept. of Nuclear Physics, Oxford, Great Britain

M.Mazzucato, M.Pegoraro, A.Peisert
Univ. di Padova, Dipt. di Fisica, Padova, Italy

M.Baubillier, J.Chauveau, W.Da Silva, J.F.Genat, F.Rossel
LPNHE, Univ. Paris VI-VII, Paris, France

T.Adye, R.Apsimon, J.Bizell, L.Denton, G.E.Kalmus, J.Lidbury, P.Seller, M.Tyndel
Rutherford Appleton Lab., Chilton, Great Britain

W.Dulinski, D.Husson, A.Lounis, M.Schaeffer, R.Turchetta
LEPSI, IN2P3/ULP, Strasbourg, France

R.Brenner, E.Sundell
Åbo Akademi, Dept. of Physics, Turku, Finland

Abstract

The DELPHI Microvertex Detector, which has been in operation since the start of the 1990 LEP run, consists of three layers of silicon microstrip detectors at average radii of 6.3, 9.0 and 11.0 cm. The 73,728 readout strips, oriented along the beam, have a total active area of 0.42 m^2. The strip pitch is 25 μm and every other strip is read out by low power charge amplifiers, giving a signal to noise ratio of 15:1 for minimum ionizing particles. On-line zero suppression results in an average data size of 4 kbyte for Z^0 events.

After a mechanical survey and an alignment with tracks, the impact parameter uncertainty as determined from hadronic Z^0 decays is well described by $\sqrt{(69/p_t)^2 + 24^2}$ μm, with p_t in GeV/c. For the 45 GeV/c tracks from $Z^0 \rightarrow \mu^+\mu^-$ decays we find an uncertainty of 21 μm for the impact parameter, which corresponds to a precision per point of 8 μm. The stability during the run is monitored using light spots and capacitive probes. An analysis of tracks through sector overlaps provides an additional check of the stability. The same analysis also results in a value of 6 μm for the intrinsic precision of the detector.

Contents

1 Introduction

The aim of a vertex detector is to provide high precision measurements of the position of particles close to the primary collision point, allowing accurate track reconstruction and precise extrapolations to the interaction region. This facilitates the reconstruction of the decay chain through the identification of primary and secondary vertices.

In this article the Microvertex Detector constructed for the DELPHI experiment is described. DELPHI is one of the four multi-purpose detectors installed at the LEP accelerator at CERN. It is used to study e^+e^- interactions at energies close to the mass of the Z^0 boson. More information about the DELPHI detector can be found elsewhere [1].

The Microvertex Detector provides high precision measurements in the plane transverse to the beam [1]. A part of the detector was tested during the start-up of LEP in 1989. A two layered detector was completed and installed for the data taking in 1990. It was upgraded to the present three layered detector with a smaller beam pipe for the 1991 data taking period. About 130,000 hadronic Z^0 events were collected by DELPHI in 1990 and 280,000 in 1991.

1.1 Physics Motivation

Since the first observations, in the 1970-ties, of the τ lepton , the J/ψ meson containing the c quark and the Υ meson containing the b quark, physics related to the third family has been of special interest.

LEP is very well suited to explore this field. Z^0s are produced with a high cross section and decay into $b\bar{b}$ in 15.4% of events, into $c\bar{c}$ in 11.9% and into $\tau^+\tau^-$ in 3.3%. In addition, the combinatorial background is relatively low compared to that found in hadronic heavy quark production.

The τ lepton and hadrons containing heavy quarks have short lifetimes. Typical values measured are (2 - 15) $\times 10^{-13}$ seconds. At LEP energies this corresponds to distances between the primary interaction vertex and the decay vertex of heavy hadrons of a few millimeters.

The presence of one or more decay vertices close to the interaction point is by itself a tag for the decays of Z^0 to heavy quarks. The vertex detector is used to recognize such topologies. It provides precise measurements of the tracks position and direction immediately outside the beam pipe of the collider. Using these values the trajectory of a track can be extrapolated back to the primary interaction point allowing the reconstruction of both primary and secondary vertices. It is illustrated in Fig. 1a which shows an event display of a candidate for the decay $Z^0 \rightarrow b\bar{b}$. A magnification of the area around the interaction region is displayed in Fig. 1b showing the ability of the Microvertex Detector to clearly separate primary and secondary vertices.

The high precision measurements of the track parameters allow an exploration of the spectroscopy, lifetimes and decay modes of the heavy hadrons. In addition to secondary vertex identification and reconstruction the precision on the effective mass determination is improved due to the improved momentum resolution. Both these effects considerably reduce the combinatorial background and improve the signal/background .

[1] R,ϕ,z define a cylindrical co-ordinate system, $+z$ being coincident with the electron beam, R, ϕ defined in the transverse plane

Results already obtained from the analysis of data taken in 1990 and 1991 highlight some of the advantages outlined above, and confirm the usefulness of the Microvertex Detector for the DELPHI experiment. Physics measurements made using the 1990 data which depend crucially on the presence of the Microvertex Detector are the measurement of the lifetime of the τ lepton [2] and of the average lifetime of B hadrons [3]. The analysis of the data taken in 1991 with the upgraded Microvertex Detector is still being performed but already some results have been obtained. Evidence for B_S^0 production [4], and a clear D meson signal accompanied by a high p_t lepton has been obtained by studying the invariant mass of $Kn\pi$, n=1,2,3, systems in hadronic events [5]. The importance of the Microvertex Detector in this latter analysis is in suppressing the background by demanding a good decay vertex separated from the primary vertex, and in improving the momentum resolution.

1.2 Design Optimization and Constraints

In the design of the Microvertex Detector, the quantity of most interest is the accurate extrapolation of a given track to the vertex region and subsequently the precise reconstruction of vertices. The Impact Parameter is defined as the distance of closest approach of a given track to the primary interaction point [2]. For tracks coming from the primary vertex it should be zero, but resolution effects smear this. These are of two types. Firstly multiple scattering in any material in front of the measured points limits the resolution especially for low momentum tracks. Secondly, any uncertainties in the track reconstruction due to the intrinsic resolution of the subdetectors used in the track fit [3] limit the precision especially at higher momentum. The impact parameter resolution is often parameterized as the quadratic sum of these two terms

$$\sigma_{IP}^2 = \sigma_{asympt}^2 + (\frac{\sigma_{ms}}{p_t})^2 \qquad (1)$$

with transverse momentum p_t measured in GeV/c.

The optimization of the Microvertex detector is achieved by minimizing the material in front of the detector, by measuring the first point precisely, as close as possible to the interaction region, and finally by having adequate angular resolution [6]. In practice this demands the use of silicon microstrip detectors with an intrinsic measurement precision of better than 5 microns.

The design of the 1990 Microvertex Detector of DELPHI was constrained by the small amount of space available between the aluminium LEP beam pipe of inner radius 7.8 cm and thickness 1.2 mm. and the DELPHI Inner Detector.

With the two layers of the Microvertex Detector placed at radii of 9 and 11 cm, σ_{asympt} was measured using di-muon events[2] to be 80 μm, while the multiple scattering term was $120/p_t$. For the 1991 running, a new beam pipe made of beryllium was installed with an inner radius of 5.3 cm and thickness 1.45 mm. This allowed a third layer to be added to the Microvertex Detector at an average radius of 6.3 cm, thus reducing σ_{asympt} to 24 μm and the multiple scattering term to $69/p_t$ μm.

[2]It is signed according to the geometric convention, that is, it is given a plus or minus sign depending on whether an observer standing at the interaction point facing the direction of the track, sees it on her right or left.

[3]The tracking detectors at DELPHI consist of the Microvertex Detector between radii of 6 and 11cm, the Inner Detector between 12 and 38cm, the Time Projection Chamber between 39cm and 120cm and the Outer Detector between 200 and 205 cm. Further Details can be found in [1].

1.3 General Layout

A brief overview of the DELPHI Microvertex Detector is given here as an introduction to the detailed description of all its components and performances given in the following sections. A schematic perspective view of the detector is presented in Fig. 2a and in Fig. 2b is shown its projection in the plane transverse to the beam.

Three concentric shells of silicon microstrip detectors at average radii of 6.3, 9 and 11 cm cover the central region of the DELPHI detector, and surround the beam pipe. The two shells at the larger radii, called the Inner and the Outer, had been completed for the LEP running period in 1990 while that at the smallest radius, called the Closer, was added for the running in 1991. The Closer shell is 22 cm long, while the Inner and the Outer are 24 cm long.

Each shell consists of 24 modules with about 10% overlap in ϕ between the modules (see Fig. 2). Each module consists of 4 silicon detectors , with strips parallel to the beam. Detector pairs are wire-bonded in series and read out at either end.

The silicon microstrip detectors with integrated coupling capacitors and biasing resistors are novel and were developed specifically for DELPHI [7]. They are 285 μm thick and have a diode pitch of 25 μm with a readout pitch of 50 μm. The number of read-out strips totals 73,728. A detailed description of the detectors performance and of the applied acceptance criteria is given in section 2.

The VLSI readout electronics produced in 3 μm CMOS, contain 128 analog channels with serial read-out. The readout chips are bonded channel by channel to the strips at both ends of the detector modules which are stiffened by a carbon-fibre support. The components of the modules and their assembly are described in section 3.

The outer ends of each module are mounted on to two aluminium semi-circular rings which surround the beam pipe. The mechanical structure is water cooled to guarantee good thermal stability. Before installation the relative alignment of the modules was surveyed using a three dimensional measuring machine, to a global accuracy of about 20 μm. The whole detector can be slid into position around the interaction region on rails fixed to the Inner Detector. The half-shells assembly, survey, electronics and detector insertion are described in section 4.

The outputs of six chips from the Closer shell, or of four chips from the Inner shell and five chips from the Outer shell are multiplexed together in electronics mounted nearby, giving 768 or 1152 channels per readout line. These signals are analyzed on-line by DSP processors in dedicated Fastbus modules. Section 5 contains the description of our data acquisition system, DSP processing and on-line monitoring.

Three methods are used to monitor any movements of the detector after its installation: a series of light spots, a system of capacitive probes and tracks passing through the overlaps between neighbouring modules. The details are given in section 6.

Both the detector alignment, internal and external, and the efficient association of the Microvertex Detector hits to the tracks reconstructed by the other tracking detectors of DELPHI are essential for satisfactory performance. Section 7 describes the procedures followed.

A detailed study of the detector performance has been made using the data collected in 1991. Section 8 provides details of the efficiency, intrinsic precision, impact parameter and two-track resolution of the detector.

Finally a summary is presented in section 9.

2 Silicon Microstrip Detectors

Each detector has a sensitive length of 52 mm for the Closer shell and 59 mm for the Inner and the Outer shell. The width of the detector changes from 19.2 mm (384 read-out channels) for the Closer shell through 25.6 mm (512 channels) for the Inner shell to 32 mm (640 channels) for the Outer shell.

2.1 Integrated Coupling Capacitors and Biasing Resistors

Silicon detectors with integrated coupling capacitors and biasing resistors [4] are used in the DELPHI Microvertex Detector [7]. The detectors are made on n-type silicon of a resistivity of 4.5 kΩcm to 5.5 kΩcm and deplete between 50 V and 60 V. The lattice orientation is (111). The diodes are formed by diffusion of boron atoms to a concentration of about 10^{18} atoms/cm^3. The diodes are 7 μm wide and are spaced every 25 μm. A layer of silicon dioxide, 0.23 μm thick, is grown during the diffusion, forming the coupling capacitor (see fig. 3). Every second strip has a metal readout line which makes a readout pitch of 50 μm.

The biasing voltage is applied to the diodes through individual polysilicon resistors. Figure 4 shows a cross section of the silicon detector along a strip and its resistor. The p^+ diffusion line, silicon dioxide and the readout strip are shown. At the end of the diffusion line there is an opening in the coupling oxide where the diode and the resistor make contact. The contact hole is metallized, which makes it possible to measure the resistance of the polysilicon lines and the coupling capacitance. It is also used to check for low resistance connections between the aluminium readout lines and the implanted diodes, called pinholes. All the polysilicon resistors are connected to a common bias line, the bias strip, which runs around the detector.

Figure 5 shows the top view of a silicon detector. The wide line, a guard ring, between the bias line and the strips is a diffusion line, whose purpose is to define the field and to collect the leakage current from the edge of the detector. Every readout line has four bond pads, two at each end, which serve to bond the first detector to the second detector and to the electronics. The reserve set of bond pads is used in case of an unsuccessful first bonding.

2.2 Acceptance Criteria and Tests

In order that the leakage current and the biasing resistors do not add more than 1000 electrons ENC the values accepted were 10 nA/strip i.e. 7 to 12 μA total and more than 1 MΩ for the resistance. To ensure good charge collection and no capacitive losses to the neighbouring strips the lower limit for the coupling capacitance was set to 7 pF/cm. The application of these criteria to the Inner layer detectors is shown in figures 6 and 7. Figure 6a shows the leakage current measured on 200 silicon detectors. Most of the detectors satisfied the specifications. Figure 6b shows the distribution of polysilicon resistors measured on the same sample. Some of them are below the design limit of 1 MΩ, but were accepted because of the deadline for assembling and inserting the Microvertex Detector in DELPHI. Figure 6c shows the coupling capacitance also measured on the Inner layer silicon detectors. All detectors passed this acceptance test.

[4] The detectors were produced by the Center for Industrial Research, Oslo, Norway.

Although pinholes in the coupling oxide are not lethal for the operation of single sided silicon detectors, they reduce the dynamic range of the electronics and should be avoided. The specifications stated that no more than 3 pinholes per detector are accepted. The distribution of the number of pinholes is shown in fig. 7a.

In addition to good spatial resolution a high detection efficiency is an important feature of the Microvertex Detector. It is obtained by ensuring that the active elements have no defects. Defects like interrupted strips or biasing resistors make an area of the silicon detector inactive. Connections between strips or resistors on the other hand degrade the position measurement, because the collected charge is spread over several channels. Defective strips were limited at not more than 1 %. This means that no more than 7, 10 and 12 defective lines on the Closer, Inner and Outer layer detectors would be accepted. Figure 7b shows the number of defective lines per detector with 1024 strips.

In total 256 silicon detectors were tested for the Inner layer and 150 passed the acceptance criteria, a yield of 57 %. Similar results were obtained for the detectors for the Outer layer produced at the same time. Detectors for the Closer layer, produced after the completion of the two others gave a higher yield of 75 % thanks to the experience acquired with the previous production.

3 Detector Modules

The basic building block of the Microvertex Detector is pictured in Fig. 8. The first photograph shows one whole module which is built out of two "half-modules", each consisting of two silicon detectors joined to a readout hybrid. A carbon fibre reinforcement profile is glued to the back of the four detectors. The second photograph is a close-up of a readout hybrid, which is a part both of the mechanical construction and of the electronic readout chain. Two screws through each hybrid attach the modules to the support structure (described in section 4). The readout chips (3, 4, or 5, depending on the layer) are glued onto the ceramic substrate of the hybrid. This substrate needs to be a good heat conductor in order to remove the heat generated by the readout chips. Each hybrid reads out two detectors with the strips connected to each other and to the amplifiers by wire-bonding. Thin flexible cables bring supply voltages and timing signals to the hybrid and take the multiplexed output signal to the outside world.

3.1 Readout Hybrid

The hybrids for the first two layers (Outer and Inner) are the same except for the width. They are made of aluminium oxide and are aligned to the paddle-wheel-shaped support rings by a smooth reference edge. The heat conductivity of aluminium oxide is 25 W/m/K. The hybrids for the third layer (Closer) are made of beryllium oxide, which has a heat conductivity of 300 W/m/K. They are aligned to the support by a bush mounted through a precisely machined hole in the hybrid. To facilitate the survey of the modules (see below), a reference cylinder is mounted on each hybrid of the first two layers. For the third layer, a reference sphere is joined with the bush.

The Closer layer hybrids are designed for double-sided silicon detectors. In order to decrease the number of lines going to the hybrid, the timing signals are multiplexed

on one line. They are deconvoluted by a custom made chip, which is mounted on the bottom side of the hybrid. A wrap-around edge connector brings the timing signals and the supply voltages to the top side, where the readout chips are.

The readout chip is the MX3 low power charge amplifier array, which is fully described in [8]. The characteristics of this chip are summarized in Table 1. Each readout strip is connected to a charge sensitive amplifier. A schematic circuit diagram is shown in Fig. 9. Given the relatively low bandwidth required, the MX3 is able to give an adequate signal to noise ratio while dissipating less than 0.5 mW per channel. Double correlated sampling (*i.e.*, taking the difference in integrated signal before and after the interaction) is used to reduce low frequency noise pick-up. In the actual configuration – two silicon detectors connected to a hybrid – the signal to noise ratio for a minimum ionizing particle is around 15:1.

The CMOS technology assures a uniform gain among the 128 amplifiers in the chip. Injecting charge through the calibrate inputs or pulsing the detector back-plane shows that the gain variation within one chip is less than two percent. The variation from chip to chip within one production batch is of the same order of magnitude. The 128 outputs are read out serially at a rate of 2.5 MHz on a single twisted pair. Groups of chips (6 or 9) are daisy-chained to the same readout bus to further reduce the number of lines.

The MX3 radiation tolerance was investigated in some detail. The general observation was that radiation increased the measured noise values almost linearly, but the rate varied from one production batch to the other. This increase in noise was eventually understood to be caused by a worsening leakage current on the input protection FOXFET devices. The radiation dose leading to chip failure varied in the range 50–850 Gy.

Table 1: MX3 Specifications

Size	6.4 mm x 6.9 mm
Number of Amplifiers	128
Power	60 mW
Risetime (10-90)%	1 μs (BW limited)
Noise	670 + 55 e^-/pF
Readout Rate	2.5 MHz

3.2 Production of Modules

The main challenge was to build a rigid and stable structure with the introduction of a minimum of extra material. Another aim was to make the strips as parallel as possible to the z-axis (the beam direction). This is important because these detectors do not measure the z-coordinate, which is only known to a precision of 1–2 mm from the other DELPHI tracking detectors. Thus, if the strip angles were too large (more than a few milliradians from the z-axis), the high resolution in the perpendicular plane would be compromised. This leads to the requirement that the four detectors should be well aligned relative to each other and relative to the readout hybrids which are aligned to the support. The modules should also be flat.

The assembly proceeds in several steps using a series of jigs. Each jig holds two pieces (detectors or hybrids) by vacuum and allows one of the pieces to be translated and rotated in the plane of the module. The jigs are mounted on top of two perpendicular translation tables equipped with precision stepper motors. The step sizes are 10 μm along the strips and 1 μm perpendicular to the strips. A metallurgical microscope, mounted above the setup, is used to observe reference features on the detectors and the hybrids. While moving the jig using the translation tables, the relative alignment between the two pieces is checked and adjusted before they are joined.

First, two silicon detectors are joined by gluing two small silicon bridging pieces to the back side. Next, a readout hybrid is attached by gluing one edge of the detector pair directly on top of the edge of the hybrid. At this stage, the strips on the two detectors are connected to each other and to the inputs of the readout chips by a semi-automatic bonding machine. The resulting half-module is then tested electrically. This test includes a back-plane pulsing and a scan with a pulsed infrared laser spot.

Two half-modules are joined by two small bridging pieces as in the first step above. All bridging pieces are metallized on the side facing the back of the detectors, thus providing the connection for the back-plane voltage between the four detectors. The connections for the strip bias voltage and the guard ring voltage are made by wire-bonding.

To strengthen the modules and to make them easier to handle, a trapezoidal, 200 μm thick carbon fibre profile is glued to the back of the four detectors. To avoid a bimetal-like bending of the module caused by the different thermal expansion coefficients, a 2 mm wide and 300 μm thick silicon piece is glued to the other side of the carbon fibre bar. This extra silicon piece also increases the rigidity of the module by roughly a factor of 4. The complete module then undergoes final electrical tests.

The detector modules are measured using the production setup and a simple support jig. The control unit for the stepping motors is linked to a computer, which records the positions of the two translation tables. The strips on the silicon detectors are observed through the microscope and their positions determined with respect to the reference cylinders (or spheres) on the readout hybrids. A three-dimensional survey of the assembled half-shells (section 4.3) measures the cylinders, the spheres and the planes of all silicon detectors.

4 Half-Shells

To build the Microvertex Detector, the detector modules described in the previous section are assembled into two half-shells. Figure 10 shows a photograph of one half-shell with all three layers mounted. Each layer consists of twelve detector modules, which are mounted on aluminium support structures called end-rings. The modules themselves hold the two ends together. The thin flexible cables from the readout hybrids are connected to additional readout electronics mounted close to the end-rings. Cooling water flows through channels inside the end-rings and also through channels attached to the adjacent circuit boards.

4.1 Mechanical Construction

The first two layers (Outer and Inner) are supported and cooled by the same end-rings, which look like paddle wheels in order to give a small overlap between neighbouring modules. Before the mounting of modules, the two ends are held together by three precision aluminium bars. These are successively removed as the modules are mounted. The third layer (Closer) is supported and cooled by another pair of end-rings, which are aligned to the first pair using a precision jig. After an initial alignment the pairs of rings can be dismounted and then relocated using precisely machined brackets. At this smaller radius, a paddle wheel arrangement would tilt the modules too much so that tracks would no longer be incident at 90 degrees. Instead, the modules alternate between two different radii. (See Fig. 2.)

The effective thickness of each aluminium end-ring is about 5 mm. The assembled half-shell is protected by inside and outside covers made of 1 mm thick foam[5] coated on both sides with 20 μm aluminium foil.

There are five cooling channels per half-shell. These channels have an inner diameter of 3–5 mm and a typical water flow of 40 cl/min. The cooling water siphons between two reservoirs, which are both below the level of the Microvertex Detector. The whole fluid system is maintained at a slight underpressure as an insurance against leaks.

The Microvertex Detector is inserted into the DELPHI barrel between the Inner Detector and the beam pipe. Small skates made of a low friction material (Delrin) are attached to the end-rings and to the adjacent circuit boards. These skates allow the half-shells to slide into place on carbon fibre rails mounted on the inner wall of the Inner Detector. Each half-shell rests on two rails, one at the bottom and one on the side. The two half-shells are not connected in any way, and there is no contact with the beam pipe.

4.2 Readout Electronics

A functional diagram of the complete electronic readout is shown in Fig. 11. Starting from the readout hybrid, the differential multiplexed output from the readout chips is transferred by a flexible kapton cable to an analog differential line driver (NE592) on the "bendflex." This is a flexible printed circuit attached to each end of the half-shell. The signal then passes to an adjacent printed circuit board ("repeater"), where a simple emitter follower drives the signal to the counting room (a distance of about 25 m). There the analog signals are digitized and read out in the SIROCCO units (see section 5).

For the later third layer (Closer), the functions of the bendflex and the repeater were combined in a single printed circuit board attached to the half-shell. The NE592 amplifier plus emitter follower were replaced by a custom designed differential analog driver - the FDD [9].

All power supplies, monitoring electronics and control signal generators are situated in the counting room. The timing signals are derived from the standard DELPHI timing unit using a purpose-built fanout [10]. These signals go to the readout chips in the reverse direction through the repeater and bendflexes.

[5]Rohacell, Roem Schweiz Gmbh.

4.3 Survey

As a first step in the alignment of the Microvertex Detector, the assembled half-shells are measured with a 3–D survey machine [6]. Figure 12 shows a half-shell (without the readout electronics) during a measurement session. The survey machine has a mechanical arm that moves in three orthogonal directions and supports a measuring head, which is a synthetic ruby stylus mounted on a touch probe triggered by a small force (about 10 grams). The table and all supporting elements are made of granite to provide good stability. On calibration objects the specified accuracy is $(3 + d/(2 \cdot 10^5))\mu$m for a measurement of a distance d (in μm) between two points. The machine measures the planes of all silicon detectors and the reference cylinders (or spheres) on all readout hybrids. The position of the strips in the plane of a module relative to the reference objects is measured separately under a microscope (section 3.2).

Each half-shell is measured twice, since the middle layer is normally not accessible to the measuring probe. One survey measuring the first two layers (Outer and Inner) takes place when only those two are mounted. Another survey measuring the first and the third layers (Outer and Closer) is done after all three layers have been mounted. During all surveys, warm water (25 °C) circulates in the cooling channels in order to simulate normal working conditions. The two measurements of the Outer layer are overlapped and found to be consistent.

The mapping precision achieved, taking all uncertainties into account, is better than 20 μm. All the steps are described in more detail elsewhere [11]. An alignment using tracks (section 7.2) later refines the strip positions in the planes of the modules, but it is not sensitive enough to improve the radial positions. However, since the radial coordinate has less influence in the track fit, the precision of the survey is sufficient.

5 Data Acquisition

The data acquisition for the Microvertex Detector is an integral part of the DELPHI data acquisition system. Only those stages that are particular to the Microvertex Detector are described here.

5.1 Readout and On-line Analysis

Synchronously with each LEP bunch crossing (every 22 μs) the charge collected on each strip is recorded by the MX3 chips. If there is no DELPHI trigger, this information is overwritten during the next bunch crossing, otherwise the next capture cycle is skipped while waiting for the second level trigger. If the event is accepted, the charge is serially read out and digitized by 36 SIROCCO Fastbus modules [7] [12]. Each SIROCCO has two independent readout units with a 10 MHz flash ADC [8] for the digitization and a Digital Signal Processor DSP56001 [9] [13] for zero suppression.

The input to each SIROCCO readout unit is one of the 72 multiplexed analog signals from the Microvertex Detector. One analog signal carries the information

[6] The Galaxy survey machine, POLI S.p.A., Varallo Sesia, Italy.

[7] Designed for the DELPHI Microvertex Detector by the CERN Electronics Division.

[8] Produced by TRW.

[9] Manufactured by Motorola Inc.

from either nine MX3 chips containing 1152 channels (Outer and Inner layers) or six MX3 chips containing 768 channels (Closer layer). At a 2.5 MHz readout speed, the digitization takes about 500 μs, after which the Microvertex Detector is ready for the next trigger. The 72 DSPs further analyse the data, compressing the 73,728 channels into typically 1,000 32-bit words for a hadronic Z^0 event or 150 words for an empty event. An event is analyzed in about 30 ms, comfortably faster than the maximum second level trigger rate of 5 Hz.

In order to find the channels with interesting data, it is necessary to evaluate three quantities: the individual channel pedestal, the common noise and the individual channel noise. The channel pedestals and the common noise are subtracted from the data, and the RMS of the channel noise is used as a reference for distinguishing true signals from background noise. All three quantities are recorded together with the data and used in the on-line and off-line monitoring.

The channel pedestals are assumed to be constant or slowly changing. The values are continually updated using a running average technique, where the new pedestal value is equal to $(1 - w_p)$ times the old value plus w_p times the channel ADC value. The weight w_p is chosen to be 1/32, which updates the pedestals sufficiently fast, while still being relatively insensitive to noise fluctuations.

The common noise is evaluated for each MX3 chip. It is calculated every event by averaging over all channels belonging to the same chip. The individual channel signal is then obtained by subtracting the channel pedestal and the common noise from the ADC value.

The RMS of the individual channel noise is also updated continually via a running average technique. The new RMS value squared is equal to $(1 - w_n)$ times the old value squared plus w_n times the signal squared, where w_n is chosen to be 1/1024. The channel signal to noise ratio is equal to the channel signal divided by the RMS noise.

A cut is made by demanding that the sum of the signal to noise ratios of two neighbouring channels be greater than 6. Only channels that satisfy this cut, and a few of their neighbours, are kept. This was shown to work well since events without tracks had typically three noise hits, while for tracks passing through the detector the efficiency was close to 100%, as will be discussed in section 8. True signals have their charge spread over two or three channels with the sum of signal to noise ratios peaked around 15.

The data records produced by the SIROCCO modules are read out by the DELPHI data acquisition system and written to cassette together with records from the other DELPHI sub-detectors.

5.2 Monitoring

The data quality is monitored on-line with an event display and a monitor program. The event display shows a single selected event. It gives a global view of the hits registered by the Microvertex Detector (Fig. 13a) and can also show detailed information for any of the clusters (Fig. 13b).

The on-line monitor analyses the Microvertex Detector data and fills a series of histograms which allow the detector performance to be evaluated. There are histograms with, for example, pedestal and noise values, signal to noise ratios and the number of clusters. A simple event reconstruction provides track segments, track

residuals and a vertex position. Some of these quantities not only check the data from the Microvertex Detector, but also give DELPHI valuable information on the running conditions. The number of clusters per event, for example, is a good monitor of the beam background, and the average position of the reconstructed vertices is an estimate of the beam position.

6 Mechanical Stability

The mechanical stability of the Microvertex Detector during data taking is essential, since a 1° C temperature change expands the support structure by 5 μm, an amount comparable to the intrinsic precision of the detector. The end-rings are made of aluminium, chosen for its ability to transmit heat, through which water is circulated, removing the 70 W generated by the readout electronics and stabilizing the temperature to 0.3° C. Temperature fluctuations are measured by resistive thermometers located at two points on each end-ring, and provide measurements accurate to 0.2° C once a minute. Two dedicated position monitoring systems measure any movements of the Microvertex Detector with respect to the Inner Detector and are described below. Movements internal to the Microvertex Detector are investigated by an offline software analysis.

6.1 Capacitive Probe Position Monitoring

A series of capacitive probes [10] are mounted at the top and side of the Microvertex Detector's end-rings and on the inside wall of the Inner Detector [14]. The probes measure the capacitance, using a 15 kHz signal. Three distinct geometries measure the gap between the two detectors: radially via 8 probes, two on each of the four end-rings; laterally through a similar set; and longitudinally, along the beam axis, through one probe on each half-shell. The radial gap can be measured with a precision of better than 1 μm while the other probes are sensitive to 10 μm movements. The capacitive probe data is recorded every minute by the detector monitoring system which also reads out the thermometer values. This is done independently of the DELPHI data acquisition and necessitates an offline correlation of the probe values with the DELPHI data.

6.2 Light Spot Position Monitoring

The second position monitoring system uses a series of light spots which shine on the Outer layer of silicon detectors. Infrared light from a Gallium Arsenide laser with a wavelength of 904 nm [11] is transported from a laser diode situated outside the detector by 48 10 m long 100 μm diameter optical fibres. The light is focussed onto the detectors using small lenses and prisms [12]. Four light spots shine on every second Outer layer module; two doublets on either end, one with the beam perpendicular to

[10] A commercially available capacitive probe readout system manufactured by CAPACITEC Inc., 87 Fitchburg Rd., Ayer MA, 01432, USA.

[11] SG 2001 A.

[12] A lens-prism combination manufactured by Fisba Optik, CH-9016 St. Gallen, optical fibres by Cableoptic S.A., CH-2016, Cortoillod and custom ordered fibre positioning guides produced by Technika Grenchen, Geneva.

the silicon, the other inclined at a 28° angle with respect to the normal. In principle, these allow a decoupling of radial and tangential module motion. In practice, we observe only small shifts (see below) and hence the differential movement between perpendicular and inclined light spots has not been observed.

The light diodes are pulsed every 64th beam crossing, thus merging light spot measurements with e^+e^- collisions. The 1 kHz rate is limited by the light diode recovery time but still provides sufficient overlap between light diode flashes and triggered DELPHI events. A single light flash provides a 5 μm measurement which averaged over an hour of data taking determines the tangential module position relative to the Inner Detector to about 1 μm.

6.3 Calibration and Results

Both of these systems were calibrated in-situ. The detector was heated by reducing the water flow in the cooling system, thereby causing the end-rings to expand. Figure 14 shows the end-ring temperature variation during this one hour test. For comparison is plotted a radial gap measurement (capacitors) and a tangential module position (light spots) during this same period. The correlation is clear.

Over the 9 months of data taking in 1991, no motion in excess of 10 μm was observed, however steady drifts of 5 to 7 μm are seen over a period of weeks (see fig. 15). Considerable jumps (20 to 30 μm) can occur outside of data taking when the detector was switched off or DELPHI was opened for repairs, but the modules return to their original position on the resumption of stable operation. At the few micron level, hysteresis and un-correlated behaviour on neighbouring detectors make it impossible to infer the position of modules which are not monitored with a light spot. Thus this information is not used in a time dependent alignment of the detector but rather to signal the presence of large shifts and identify stable periods of operation.

6.4 Position Monitoring with Tracks

The stability of the detector was monitored using tracks which pass through the overlap regions, both of neighbouring modules within a half-shell and of the overlaps occurring between the two half-shells. Charged tracks from hadronic Z^0 decays passing through overlaps having at least three hits and a minimum transverse momentum of 0.5 GeV were used. A circle fit was made through any two hits taking the curvature from the external tracking, and the distance of other hits from this track was calculated. The variation of this residual provides a measurement of the detector stability. Under typical running conditions there are 50 tracks/day/overlap which provide a measurement accuracy of better than 2 μm.

During the 1991 data taking period the contribution to the precision from mechanical instabilities is estimated to be less than 3 μm. The overlaps between the two half-shells (Fig. 16a) behave no differently than those within the same half shell (Fig. 16b). The average RMS of the 1991 residual distributions of all overlaps was less than 2 μm (Fig. 16c).

7 Offline Reconstruction and Alignment

As described in section 5.1, only clusters with a signal larger than six times the single channel noise were written to cassette. The off-line analysis starts by calculating the position of each cluster in the local coordinate system of a singe silicon detector. This one-dimensional position is the pulse height weighted average of the strip with the largest pulse height and its largest neighbour. The analysis then proceeds by associating the Microvertex Detector clusters with tracks found in the rest of the DELPHI tracking detectors. The z coordinate from the associated track is used to correct each cluster position for the effect of any small angle between the strips and the z axis. Associated and corrected hits are then included in a final track fit. This section describes the association between tracks and clusters and the detector alignment using tracks. More detailed cluster studies are presented in section 8.

7.1 Association

As indicated above, tracks are first found without using the Microvertex Detector. In a second stage, the tracks are extrapolated to the three silicon layers and associated with the clusters. If the external track extrapolations were accurate enough, on the order of the readout pitch (50 μm), the track-cluster association would be straightforward. There would be at most one possible cluster per layer. Unfortunately, the track extrapolation precision will never reach that level. The typical uncertainty on these extrapolations was 250 μm, but has recently been reduced to 150 μm. This improvement arose using the Microvertex Detector to calibrate the other tracking detectors. The large track extrapolation uncertainties create ambiguities in the association of clusters to tracks in events with a high track density. Both in jets and three-prong tau decays, for example, it is very common to have two tracks separated by less than one millimeter at the radius of the Microvertex Detector.

With the track uncertainties and track density indicated above, it is clear that we cannot expect to make a unique association in each silicon layer separately. But by using all three layers together, we can eliminate many of the ambiguities. The procedure starts by setting a window around a track in the first (Outer) layer. The size of this first window depends on how well the track position at the Microvertex Detector was determined by the external track fit and is typically of the order of one millimeter. For each cluster found within the window, the track is forced through that cluster and extrapolated to the next silicon layer, where a more narrow search window can be used. The size of this second window depends on how well the track angle is known from the external fit and, for low momentum tracks, on the expected amount of multiple scattering. If a cluster is found in the second layer, the track can be forced through two clusters and extrapolated to the third (Closer) silicon layer. At this point, the uncertainties on the original track are virtually eliminated, and a possible third cluster is required to lie within a very narrow window with a full width of one to two hundred microns.

This sequence of tighter and tighter cuts removes most of the ambiguities in the track-cluster association. Figure 17 shows the fraction of tracks that are uniquely associated to clusters, as a function of the track multiplicity, in the fifteen-degree sector to which the track belongs. In hadronic Z^0 decays, the most populated sector typically has a track multiplicity of four or five. The figure shows how the number

of ambiguities is successively reduced by the second and third layers. Having no ambiguities for a track does not necessarily mean that the association is correct, but it is a good start.

A non-negligible fraction (about 15 %) of the external tracks have much larger uncertainties than the typical ones given above. Many of these tracks can be correctly associated to clusters by doing a second pass with much looser cuts in the first and second layers. The cut in the third layer remains the same, because it does not depend on the external tracking. The looser cuts do not create many ambiguities, since most of the clusters are already associated to other tracks. Because of inefficiencies in the Microvertex Detector, some tracks do not find clusters in all three layers, in which case the association is less reliable. It is also possible for a track to find more than three clusters (up to a maximum of six) if it goes through an overlap between two sectors.

7.2 Alignment

The starting point for a software alignment of the Microvertex Detector is the mechanical measurement, in which the relative module positions in the same half-shell are known with an accuracy of 20 μm.

There are two steps to the software alignment procedure. In the first step, we align the two half-shells relative to each other with a precision of 10 μm and position the complete detector within the DELPHI reference frame. In the second, we improve the module positions within the detector using a minimization procedure which is internal to the Microvertex Detector. The remaining systematic uncertainties are of the order of 5 μm.

7.2.1 External Alignment

The Outer Detector, built of 24 planks of drift tubes with an intrinsic measurement precision of 100 μm and an overall alignment precision of 700 μm at a radius of two meters defines the DELPHI reference frame.

The alignment uses 2000 di-muon events with hits in the Microvertex and Outer Detectors. Viewed in the $R\phi$ plane, a muon pair describes the arc of a circle, neglecting initial and final state radiation effects. The Outer Detector hits define a circle, with a curvature calculated from the beam energy and the polar angle. The residuals between the Microvertex hits and the circle are minimized by considering translations in the x and y coordinates (there being no z measurement in the Microvertex Detector), and three rotations. In this way, we place each half-shell in the centre of DELPHI with an accuracy of 30 μm.

Further improvement in the orientation of each half-shell is obtained as follows. With an effective resolution for di-muon events of 700 μm at a distance of two meters from the interaction region, the Outer Detector determines the muon direction at the Microvertex Detector with an accuracy of 0.3 mrad. Imposing this constraint on each muon improves the orientation of each half-shell. Furthermore, each di-muon event can be forced through the Outer layer of the first half-shell with the track direction as given by the Outer Detector. By minimizing the hit residuals in the second half-shell to this track, we place the two half-shells, relative to each other, to better than 10 μm.

After this first step, the position of each module in the frame of each half-shell is known to 20 μm. The position of each half-shell in the frame of the Microvertex Detector is known to 10 μm, and the position of the Microvertex Detector in the DELPHI frame is known to 30 μm.

7.2.2 Internal Alignment

In the second step, two techniques are used to align the individual modules of the Microvertex Detector.

The first technique uses the di-muons again. A least squares fit is made for each di-muon, with the uncertainty on each Outer Detector point set at 700 μm, and on each Microvertex Detector point at 8 μm. Two translations and a rotation per module minimize the hit residuals to this constructed track. The translations are along the module plane (thus approximating an $R\phi$ shift), normal to the plane (thus approximately an R shift) and a rotation in the plane. There is no sensitivity to movements in z, and very little to rotations out of the plane.

The second technique uses hadronic events. On an event-by-event basis, all tracks with momentum greater than 1 GeV/c having a hit in each layer of the Microvertex Detector are considered. We extrapolate these to the interaction region and find a common vertex. The uncertainty on the vertex and the chi-squared probability are calculated. The latter is reasonably flat except for a large spike at zero. A cut in chi-squared probability at the 1% level eliminates events with secondary vertices and those with ill-measured tracks. For each track, in each event passing these cuts, we refit with the hits in the Microvertex Detector and a vertex constraint. The residuals, to each of these refitted tracks, are minimised using the same shifts and rotations per module discussed above. The shifts and rotations applied to each module are consistent between the two techniques.

The precision of the Microvertex Detector can be determined by a number of tests, the full details of which are documented elsewhere [15].
Of particular importance is the impact parameter resolution defined in equation 1. This is not measured directly because of the finite size of the interaction region, however it can be deduced from the apparent distance between the two muons in a di-muon event, both extrapolated back to the interaction region. We refer to this quantity as the "Muon Miss Distance" and plot it in Fig. 18. It can be shown that $\sigma_{MMD} = \sqrt{2}\,\sigma_{IP}$ and thus the impact parameter resolution for high momentum tracks is 21 μm. This also implies a single point precision in the Microvertex Detector of 8 μm.

Direct tests of the vertexing ability of the detector are performed in two ways. Firstly in the reconstruction of the point at which tau leptons decay into 3 charged tracks. With the Microvertex single point resolution set at the above mentioned 8 μm, and with due account being taken of multiple scattering, the chisquared probability distribution is flat showing that the resolution has been correctly estimated. Secondly from an enriched sample of Z^0's decaying to quarks u, d, s, an attempt is made to reconstruct the primary vertex. These are consistent with the centre of the beamspot within the calculated errors, and from the resulting distribution it is shown that possible systematics in the radial position of reconstructed vertices are less than 15 μm.

Moreover, several tests concerning the internal consistency of the detector are

described in section 8.3.

In conclusion, we align the modules of the Microvertex Detector with respect to each other to an accuracy of 5 μm. The detector position in the DELPHI frame is known, with an accuracy of 30 μm. Numerous tests referred to above, show the internal resolution, time averaged over the 1991 data-taking period, to be 8 μm.

8 Detector Performance

8.1 Efficiency

After the installation two detectors had electrical faults, rendering 2.3% of the channels inoperative from the start of the run. During the run a few more detectors developed problems, which were later understood to be caused by bond-wire failures, and in one case a micro-crack in the ceramic hybrid. This caused 8.5% of the channels to be dead at the end of the running period. It should be noted however that, for the whole period, at least one layer was operative for 100% of the ϕ coverage, and for 93% of ϕ there were at least two hits per track.

The efficiency, studied with tracks from the hadronic decays of Z^0s, in a fiducial area of the detector was 95.5%, 97.5% and 96.3% for the Closer, Inner and Outer layer respectively. The inefficiencies include a small contribution of the association efficiency to tracks found by the other tracking detectors in DELPHI, a contribution related to the quality of tracks and a contribution due to noisy channels in the Microvertex Detector. The first two contributions can be eliminated by calculating the efficiency for the good quality tracks from the leptonic decays of Z^0s. The corresponding numbers were 97.5%, 99.0% and 97.9%.

8.2 Cluster Characteristics

A channel is defined as belonging to a cluster if the ratio of its pulse height (PH) to its noise (N) is larger than a fraction f of the channel with the maximum PH/N in that cluster. A cluster is only accepted if the sum of the PH/N of the individual channels is larger than 6, and if there is at least one channel with a PH/N larger than 3. A value of 0.2 for the fraction f was found to give the best intrinsic precision. Notice that, as explained in Section 3.1, no gain corrections are necessary to the data.

Figure 19 shows the number of channels per cluster as a function of the incidence angle of the corresponding track with the detector in the $R\phi$ plane. As expected the fraction of 1-channel clusters decreases for increasing angle while more 3-channel clusters are found for non perpendicular tracks. Clusters with 4 or more channels are not expected for angles below 0.3 rad, and should be attributed to δ electrons, merging clusters and detector defects. Events with a hadronic decay of the Z^0 contained on average 65 clusters in the three layers of the detector. The clusters not associated with tracks have an average cluster width larger than the one for associated clusters. However they do not differ enough to distinguish them based on just the cluster size, nor does their number (3 per event) make it necessary to remove them.

The 1.23 Tesla magnetic field in DELPHI is perpendicular to the electric field in the silicon and causes the holes in the silicon to drift with a Lorentz angle α_L relative to the electric field direction. Hence a minimal cluster width will be obtained for

tracks with an angle α_L relative to the normal of the detectors in the $R\phi$ plane. The minimal cluster size (see Fig. 19) was found to correspond to $\alpha_L = 54$ mrad consistent for all detectors.

Due to the multiplexing of up to 1152 channels on one read-out line and the read-out speed, a cross-talk bias could be introduced in the clusters. To measure the size of this effect the difference in PH between the neighbouring channels of the channel with the largest PH in a cluster was determined normalized to the PH of the channel with the largest PH. This asymmetry in cluster shape is a function of the incidence angle of a track with the silicon, due to diffusion of the holes which drift to the implants. For tracks which traverse the silicon with the Lorentz angle there should be no asymmetry due to diffusion, and hence the remaining asymmetry is attributed to electronic cross-talk. The Inner and Outer modules (nine MX3-chips bussed together) showed a 4% forward cross-talk, because of the capacitive load on the output bus. For the Closer modules (six $MX3$-chips bussed together), groups of three chips were decoupled using diodes and no significant cross-talk was observed.

The full line in Fig. 20 shows the PH distribution for typical detectors, normalized to the noise of one channel. The values have been also normalized to the minimal track length of a particle traversing the silicon, which is an average correction of 15%. The most probable value of the Landau distribution is 15. The dashed line in Fig. 20 shows the PH/N distribution for clusters which have not been associated to tracks, which clearly peaks towards small values. The position of a cluster is obtained by calculating $\eta = PH(i+1)/(PH(i) + PH(i+1))$, where only the 2 channels with the largest PH are considered. Figure 21 shows the η distribution for tracks which traverse the silicon at large angles (full-line), and tracks around the Lorentz angle (dashed-line). For the latter the function of the intermediate strip, which is not read-out, can clearly be observed. Note that due to the choice of 0.2 for f (see top of this section), η is restricted to $0.17 < \eta < 0.83$. All remaining clusters contain only one channel by definition. The true illumination of detectors is uniform in η, while the η distribution shows a clear non-uniform reconstruction of the hit position. Hence the reconstructed hit position should be corrected as a function of η. These corrections are obtained by comparing the found hit position with its predicted position using the other two layers, and are shown in Fig. 22.

Due to smaller capacitance the charge loss in the intermediate strips is faster than in the read-out strips. This loss is furthermore a function of bias resistors, which vary from batch to batch, and of the integration time of the MX3 amplifier, which due to external requirements, notably to prevent pick-up of the clocking signals by the Inner Detector of DELPHI, is twice the optimal value. Fig. 23 shows the relative PH in a cluster as a function of η for the three layers. Since the distributions are symmetric around 0.5, and the total PH/N is sufficient no precision loss is expected due this PH loss.

8.3 Hit Precision

The hit precision, independent of systematic alignment errors or time instabilities, has been found to be 6 μm for tracks with an incidence angle in the silicon close to the Lorentz angle. This value is obtained by studying the overlaps between detectors in one layer, using as a pivot for the track one of the other layers. The residual distribution yields 6.1 μm for the Closer layer, where a track passes through both

detectors in the overlap with an angle within 100 mrad relative to the Lorentz angle. For the Inner and Outer layers one of the two hits considered will always be produced by a track traversing the silicon at an angle close to 250 mrad, therefore giving rise to a larger residual. However the corresponding number for these layers is 7.4 μm, assuming that both hits have equal precision. As will be shown below, this precision can be interpreted as an average of the 6 μm for tracks close to the Lorentz angle and 9 μm for tracks at the largest incident angles.

To be able to assign proper errors to the hits, and study possible systematics effect, the precision of hits has been measured as a function of the following variables: incidence angle, cluster size, pulse height, η and noise. As measure for the precision the width of the residual distribution between a track defined by Closer and Outer layers and the corresponding hit in the Inner layer is used, the Inner layer being the layer under investigation. To this residual both the precision of the track and the hit in the Inner layer contribute, and if all layers would have identical errors the corresponding single hit precision equals 0.82 times the measured residual.

Figure 24 shows the residual as a function of the incidence angle of a track at the Inner layer, showing that the best precision is obtained for tracks close to the Lorentz angle. For clusters which contain more than two channels, a cluster algorithm including only the two edge channels in the cluster has been studied. Figure 25 shows a comparison between the precision of the η algorithm including only the two largest PH in the cluster (full-line), or ignoring the centre channel for clusters which contain three channels (dashed line). Only hits in the Inner layer with three channels per cluster are included, and the width of the residual distribution is plotted as a function of the incidence angle of the tracks at the Inner layer. Only if the angles with which the tracks traverse the silicon would have been larger would the present algorithm have to be modified to gain precision. Due to the 24-fold modularity in ϕ the algorithm which uses only the two largest PH gives the most precise positions.

Figure 26 shows the residual as a function of the PH of the cluster in the Inner layer. The distribution shows that the best precision is obtained for tracks which deposit 20% more than the most probable amount of energy. The precision degrades for small pulse heights due to electronic noise. For large energy depositions a worse precision is caused by δ electrons or Landau fluctuations for non perpendicular tracks which both can pull the cluster centroid away from the track position.

Figure 27 shows the residual as a function of η. As expected the best precision is obtained when the track traverses the silicon in between the two channels which are read-out. Note that due to the cluster definition algorithm used, all η values less than 0.17 and above 0.83 produce only single channel clusters, which are put at η=0.

A study was done to identify the hit precision based on the characteristics of clusters. Clusters are put into three categories which are defined by the PH and N values of the channels in and around the cluster. Figure 28 shows the corresponding hit residual for the three categories, where it should be noted that the Closer and Outer layer hits have been selected to be of the best category. The precision ranges from 6.5 μm for 77% of the hits to 17 μm for the worst 6% of the hits.

8.4 Two-track Resolution

Figure 29 shows the probability that two tracks are each associated to two separate clusters as a function of the distance between the tracks. Fifty percent probability is

reached at a track separation of 120 μm. For this study, only two of the three layers are used in the track fit. The tracks are then extrapolated to the third layer, where the separation between pairs of tracks is calculated. The non-zero values at very small track separations are usually caused by nearby clusters which are not related to either of the two tracks (and have been mistakenly associated to one of them).

The probability that at least one of the two tracks has an associated cluster is independent of the track separation, as is the total charge associated to the two tracks. In other words, if there is only one cluster associated to two close tracks, the charge of that cluster is twice the charge from a single track. A more sophisticated cluster algorithm would be able to split some of them and to give a better two-track resolution. However, with a readout pitch of 50 μm, one does not expect to be able to go much below 100 μm.

8.5 The Impact Parameter and Its Error

As has already been described in the section on alignment, the precision at the beamspot for tracks extrapolated from the Microvertex Detector for di-muon events indicates an average error on the impact parameter, of 21 μm. This value is of course the asymptotic value, since for 45 GeV/c muons the multiple scattering contribution is negligible. The expected impact parameter error for hadronically produced tracks integrated over all angles as a function of the momentum of the tracks in the xy-plane can be described with $\sqrt{64^2/p_t^2 + 22^2}\mu$m ($p_t$ in GeV/c). A single hit precision of 8.4 μm derived from the alignment studies has been used. This value also gave a flat probability distribution for vertex fits in 3-prong tau decays. Due to the non uniform distribution of material, mainly in ϕ, and the possibility of having up to six hits in the Microvertex Detector for a single track, this representation is only an approximation made to allow an easy comparison with the data.

To test the description of the errors in hadronic events an enriched light quark sample was selected using the following procedure. An event is split in two hemispheres according to its thrust axis ($T = \mathrm{Max}(\sum_i |\mathbf{p}_i \cdot \mathbf{n}| / \sum_i |\mathbf{p}_i|)$, where T is the thrust, $\mathbf{p}_i$ are the momentum vectors of the particles and $\mathbf{n}$ is a unit vector along the thrust axis). In each hemisphere a vertex is constructed by rejecting all tracks which miss the vertex by more than five standard deviations to reject obvious outliers. Figure 30 shows the longitudinal distance between the vertices along the thrust axis for events where the combined χ^2 probability of the two vertices is smaller (full-line) and larger (dashed-line) than 10%. A clear asymmetric distribution is observed for the bad probability case, while for the complementary sample the distribution is symmetric, hence the life-time contribution to the impact parameter in this sample is suppressed. The events with the good probability are selected, and the impact parameter of each track in the event is plotted versus the vertex constructed from the remaining tracks, only accepting tracks in the vertex which lie within two standard deviations. Figure 31 shows the measured error on the impact parameter as a function of p_t (full-line), with the contribution from the vertex taken out quadratically. This vertex contribution is calculated using the expected error per track for the tracks in the vertex, and is quite small as is shown by the dashed line in Fig. 31. Parametrizing the error in the same way as for the expected distribution yields $\sqrt{69^2/p_t^2 + 24^2}\mu$m ($p_t$ in GeV/c). The dotted line gives the expected distribution as described above. This result is in agreement with the measurements from $\mu\mu$ and 3-prong tau decays.

No systematics is observed for the ϕ and θ dependence of the impact parameter error.

9 Summary

The DELPHI Microvertex Detector has operated successfully since the beginning of the 1990 LEP running period. The two layered detector used in 1990 was upgraded with a third layer and a smaller beampipe in 1991. The same detector is currently used for the 1992 run. For the 1993 run, two of the layers will be replaced by double-sided silicon detectors.

The Microvertex Detector uses 0.42 m^2 of silicon microstrip detectors with a diode pitch of 25 μm and a readout pitch of 50 μm. A characteristic feature of these detectors is the use of integrated coupling capacitors and polysilicon biasing resistors. With the requirements of a total leakage current less than 10 μA, biasing resistors with a resistance higher than 1 MΩ, a coupling capacitance greater than 7 pF/cm, and the number of defective strips less than 1%, the detector yield was 57% for the Inner and the Outer layer detectors and 75% for the Closer layer detectors.

The three layers of silicon detectors (average radii 6.3, 9.0 and 11.0 cm) cover polar angles from 43° to 137°. In this range the total amount of material traversed by a track is on average 1.5% of a radiation length. Each layer covers the full 2π of azimuthal angle, with a 10–15% overlap between neighbouring sectors. During the run, a few detector modules developed problems, but 93% (100%) of azimuthal angle remained covered by at least two (one) layers. For the remaining detector modules, the hit efficiency was 98%.

Charge sensitive amplifiers on the MX3 readout chips give a signal to noise ratio of 15:1 for minimum ionizing particles. The 73,728 readout channels are multiplexed on 72 analog differential lines, which are digitized in SIROCCO Fastbus units. These units use digital signal processors for zero suppression, which results in an average event size of 1.3 kbyte. For hadronic Z^0 decays, the average size is 4 kbyte.

Good mechanical stability is achieved by mounting the detector modules on aluminium end-rings and using water cooling to remove the 70 W generated by the readout electronics. The stability is monitored during runs by a system of light spots and a system of capacitive probes. The contribution to the precision from mechanical instabilities is estimated to be less than 3 μm from the analysis of tracks going through the overlaps between neighbouring sectors.

A survey of the Microvertex Detector before installation determines the positions of all strips with a precision of 20 μm. Further alignment using tracks reduces this uncertainty to a level that is negligible compared to the precision of the clusters. This precision is a function of many variables, *e.g.* the track incidence angle and the cluster size, but is around 8 μm averaged over all 1991 data with 95% of clusters included.

The impact parameter uncertainty has been determined from hadronic Z^0 decays, and is well described by $\sqrt{(69/p_t)^2 + 24^2}$ μm, with p_t in GeV/c. This agrees with the value of 21 μm obtained for 45 GeV/c muons from $Z^0 \to \mu^+\mu^-$ decays.

The high precision of the Microvertex Detector has been a key ingredient in the analysis of the more than 400,000 Z^0 events collected in 1990 and 1991. It has been crucial for the analyses of the tau lepton and the beauty and charm hadrons. Adding a third layer greatly improved our understanding of the detector alignment and the association of clusters with tracks. The resulting reduction of systematic uncertainties

leads to a better spatial precision and shows the advantage of three layers over two.

The operation of the Microvertex Detector has been straight forward. The detector stays on essentially for the whole year during all phases of LEP operation. The design makes it relatively insensitive to the machine background, and no damage of any kind has been observed.

Acknowledgements

The detector could only be constructed thanks to the dedicated effort of many technical collaborators in all laboratories participating in the project. We wish to express our appreciation to all of them, and in particular to M. Burns.

References

[1] P. Aarnio et al., Nucl. Instr. and Meth. **A303** (1991) 233.

[2] P. Abreu et al., Phys. Lett. **B267** (1991) 422.

[3] P. Abreu et al., Z. Phys. C - Particles and Fields **53** (1992) 567.

[4] P. Abreu et al.: Evidence for B_s^0 Meson Production in Z^0 Decays, CERN-PPE/92-104, submitted to Physics Letters B.

[5] P. Abreu et al., DELPHI Col.: A Measurement of B Meson Production and Lifetime Using Dl- Events in Z^0 Decays, paper submitted to the XXVI International Conference in High Energy Physics, DALLAS, Texas, USA, August 5-12 1992.

[6] H. Dijkstra et al., Nucl. Instr. and Meth. **A277** (1989) 160.

[7] M. Caccia et al., Nucl. Instr. and Meth. **A260** (1987) 124.

[8] J.C. Stanton, A Low Power, Low Noise Amplifier for a 128 Channel Detector Readout Chip, IEEE Trans. Nucl. Sci. **36**, 522

[9] P. Astier, J.F. Genat, J. Pelletier: A Fast Differential Cable Driver Chip, LPNHE Internal Report 92-120.

[10] G.Barichello, M.Pegoraro: Microvertex Fanout, DELPHI 90-19 TRACK 63, 12 June 1990.

[11] A. Andreazza, P. Biffi, C.Meroni, A. Stocchi, Nucl. Instr. and Meth. **A312** (1992) 431.
A. Andreazza, Thesis, Milano 1991

[12] N.Bingefors, M.Burns: SIROCCO IV - Hardware and software manual, DELPHI 88-48 TRACK 48, 8 July 1988.

[13] DSP56000/DSP56001 Digital Signal Processor User's Manual, Motorola Inc., 1990.

[14] M.Battaglia et al., Nucl. Phys. **B** (Proc. Suppl.) **23A** (1991) 448.
M. Caccia et al., Nucl. Instr. and Meth. **A315** (1992) 143.

[15] R. McNulty: The Alignment of the DELPHI Microvertex Detector, DELPHI 92-40 TRACK 69, 27 March 1992.

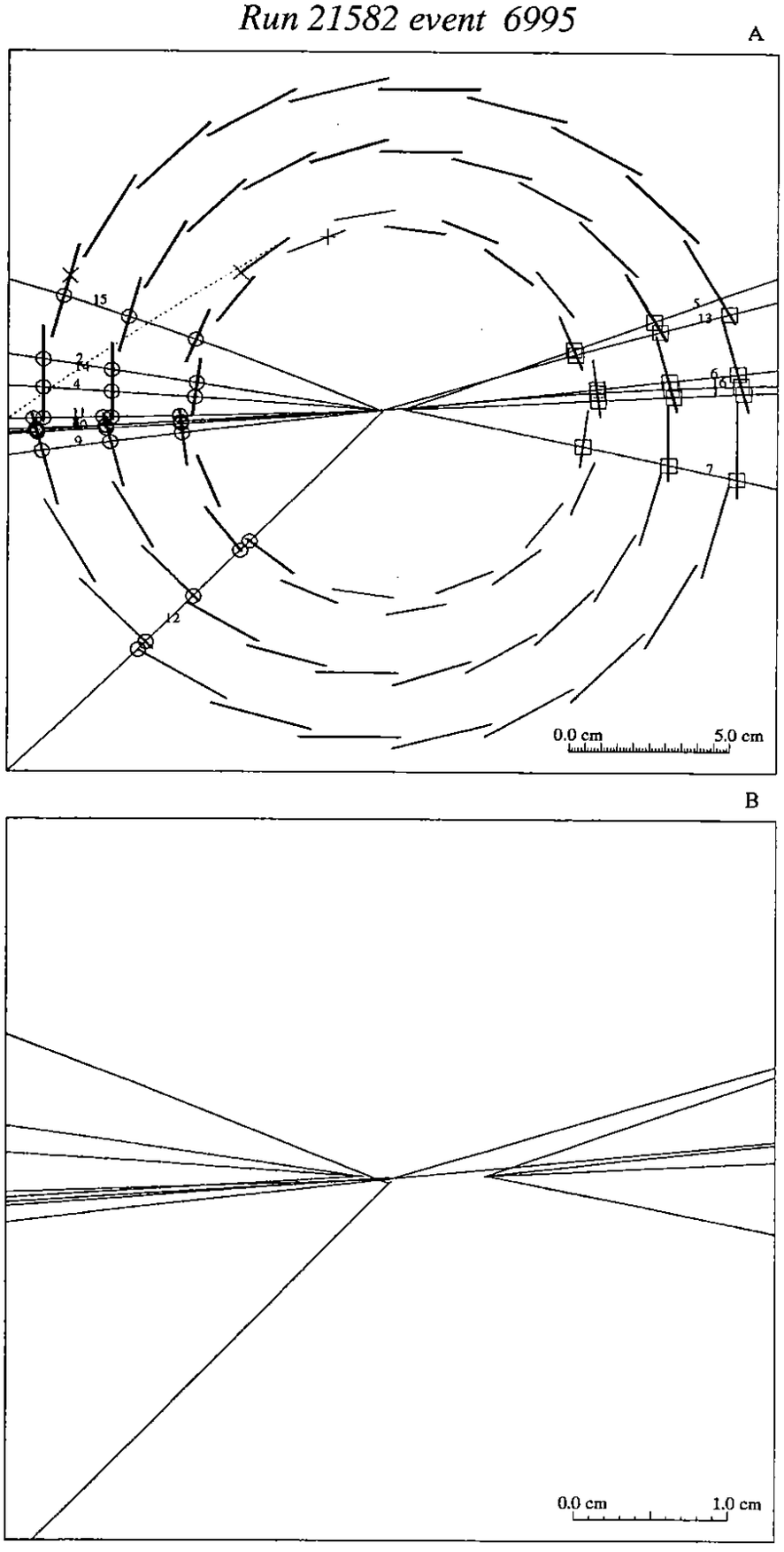

Figure 1: Event display for a $Z^0 \rightarrow b\bar{b}$ candidate.

a

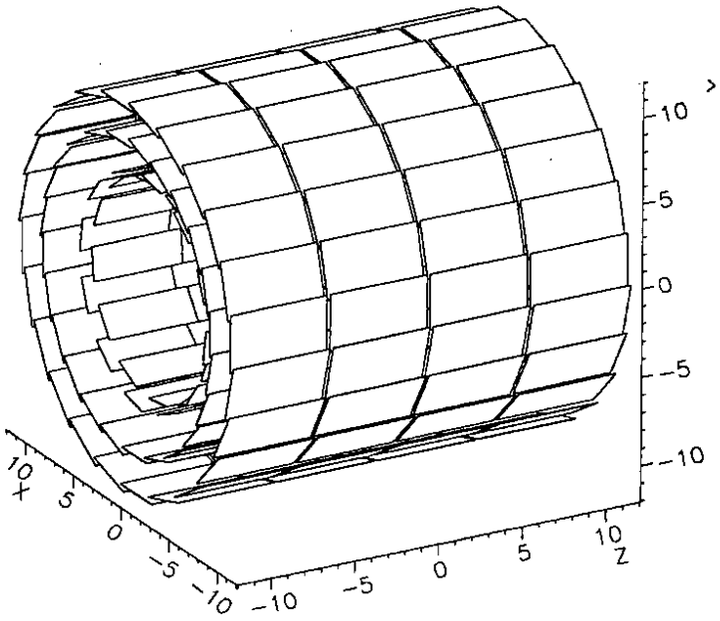

b

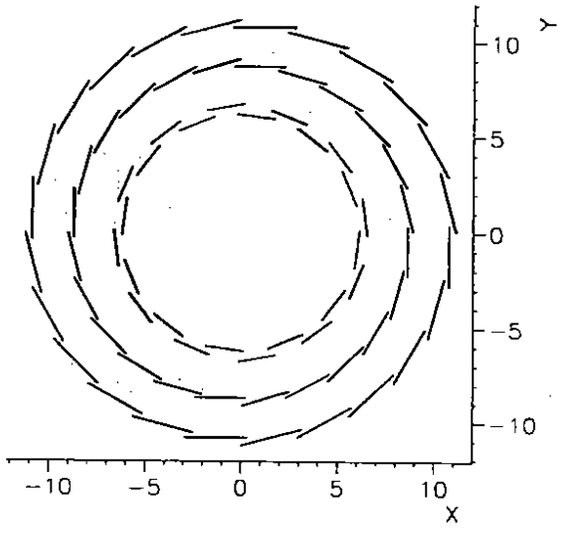

Figure 2: Schematic layout of the DELPHI Microvertex Detector: a) Perspective view. b) Projection on the plane transverse to the beam.

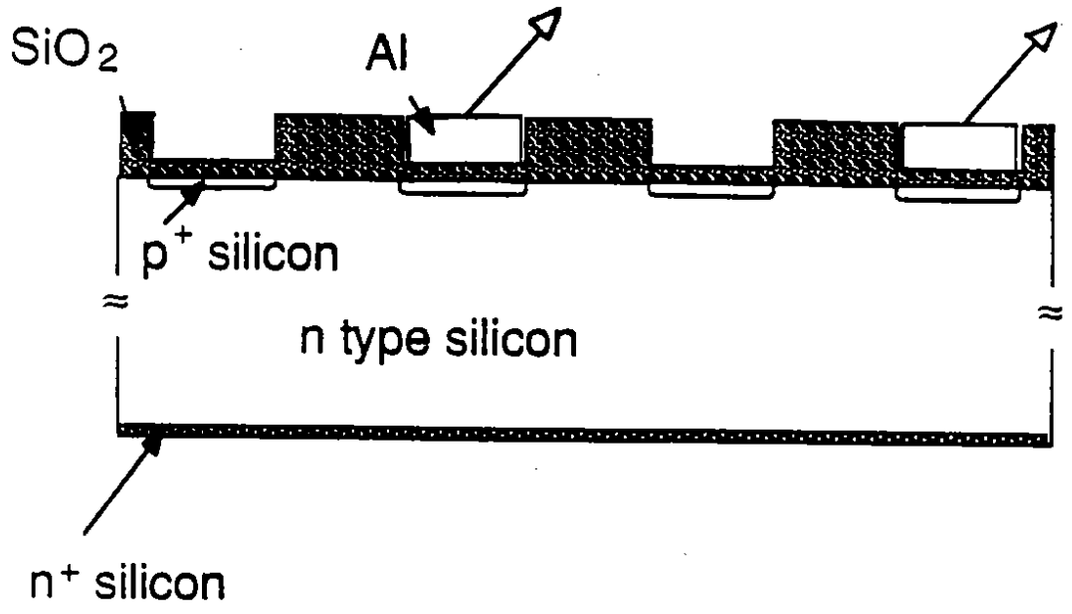

Figure 3: Cross section of a detector with integrated coupling capacitors and biasing resistors.

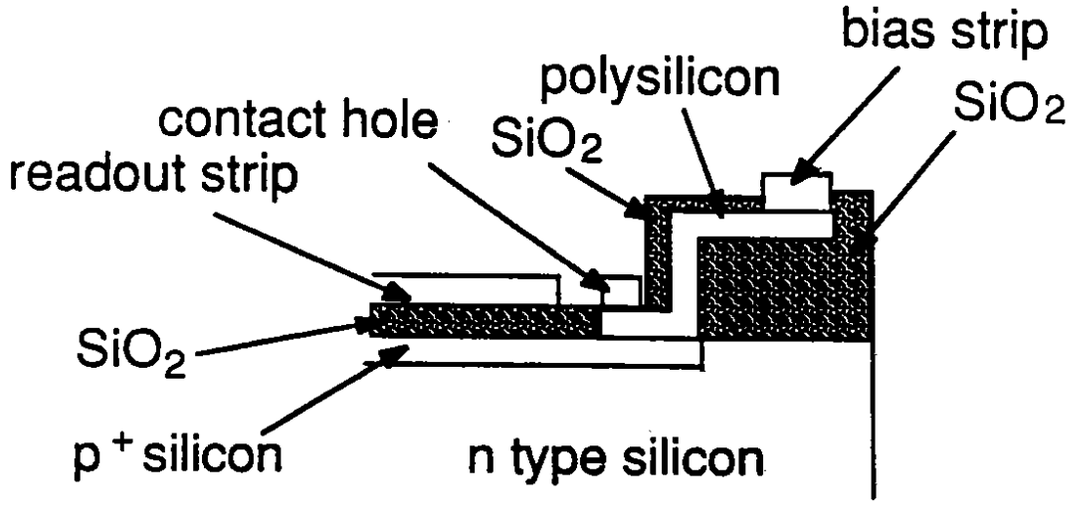

Figure 4: Cross section through a strip of a detector with integrated coupling capacitors and biasing resistors.

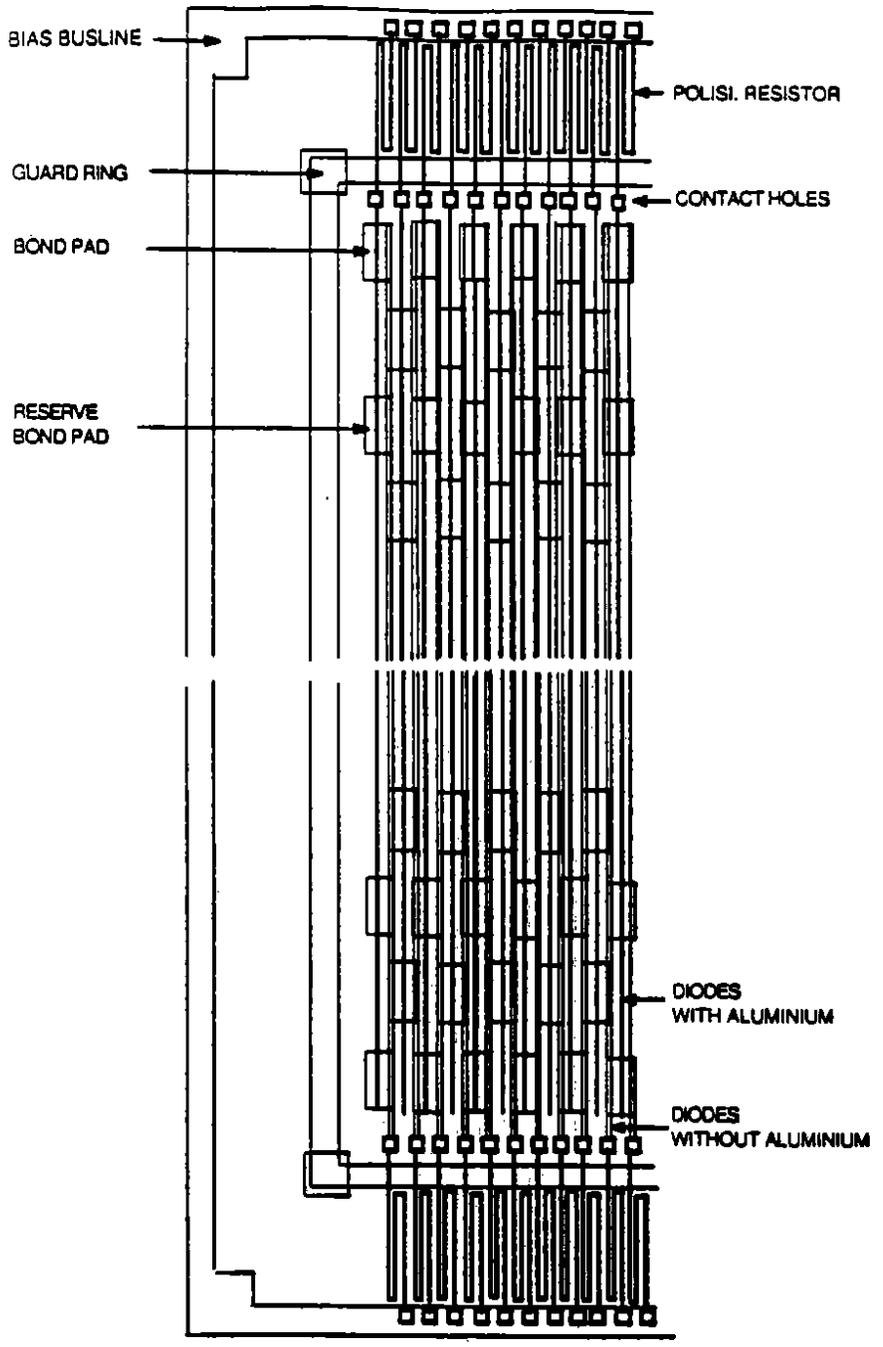

Figure 5: Top view of a detector with integrated coupling capacitors and biasing resistors.

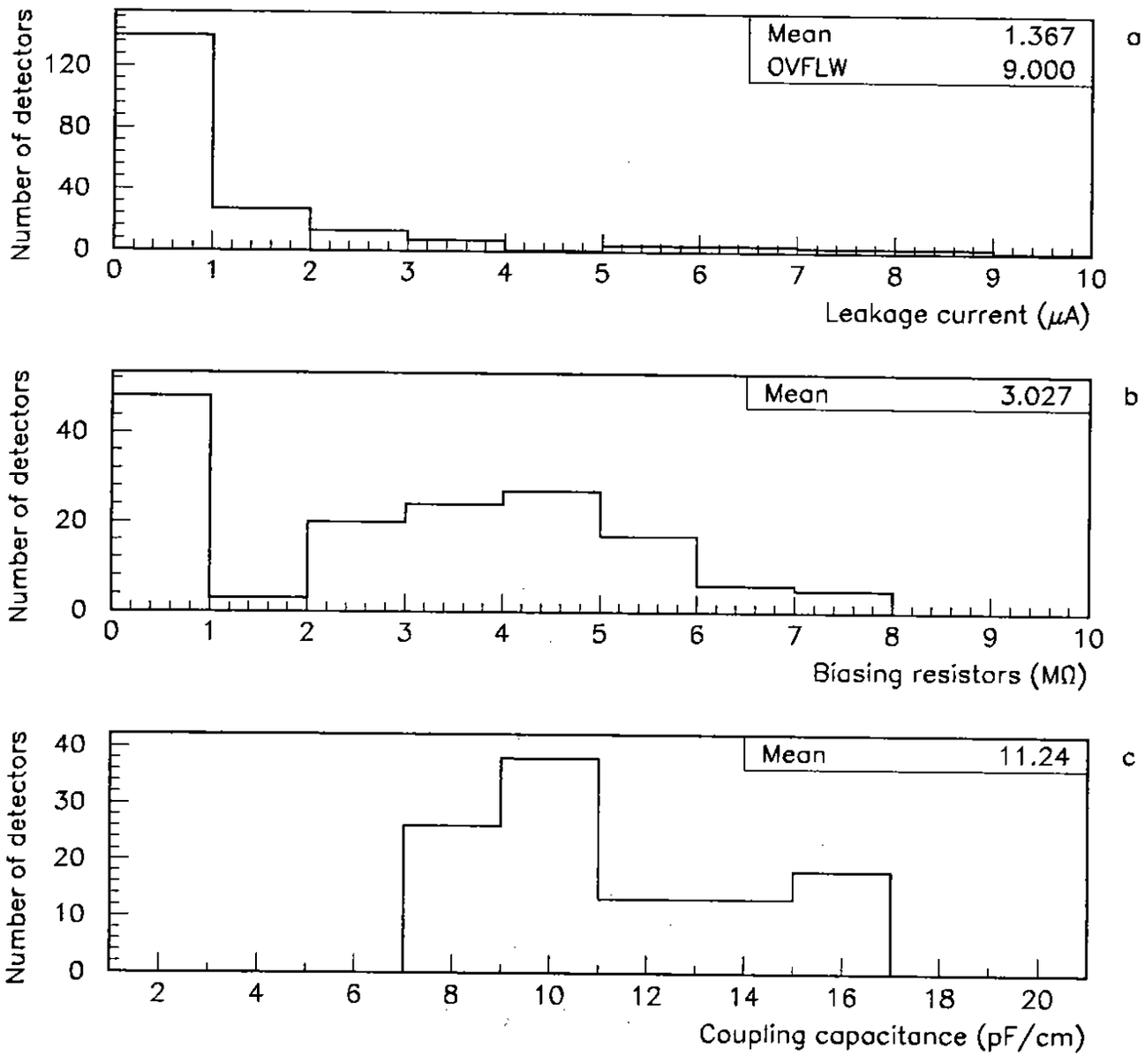

Figure 6: Results of the standard checks applied to the Inner layer detectors. a) Distribution of the leakage current. b) The biasing resistance values. c) The coupling capacitance values.

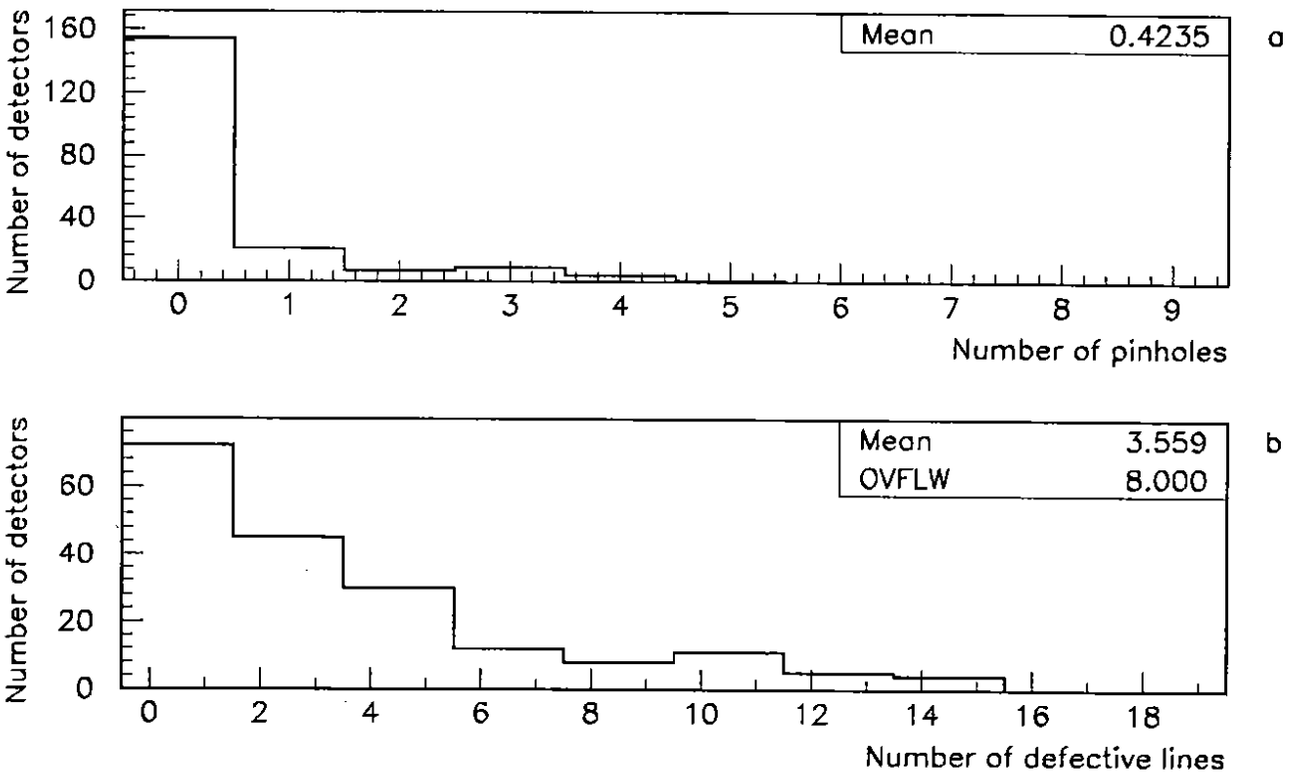

Figure 7: Further checks for the Inner layer detectors. a) The number of pinholes. b) The number of defective strips.

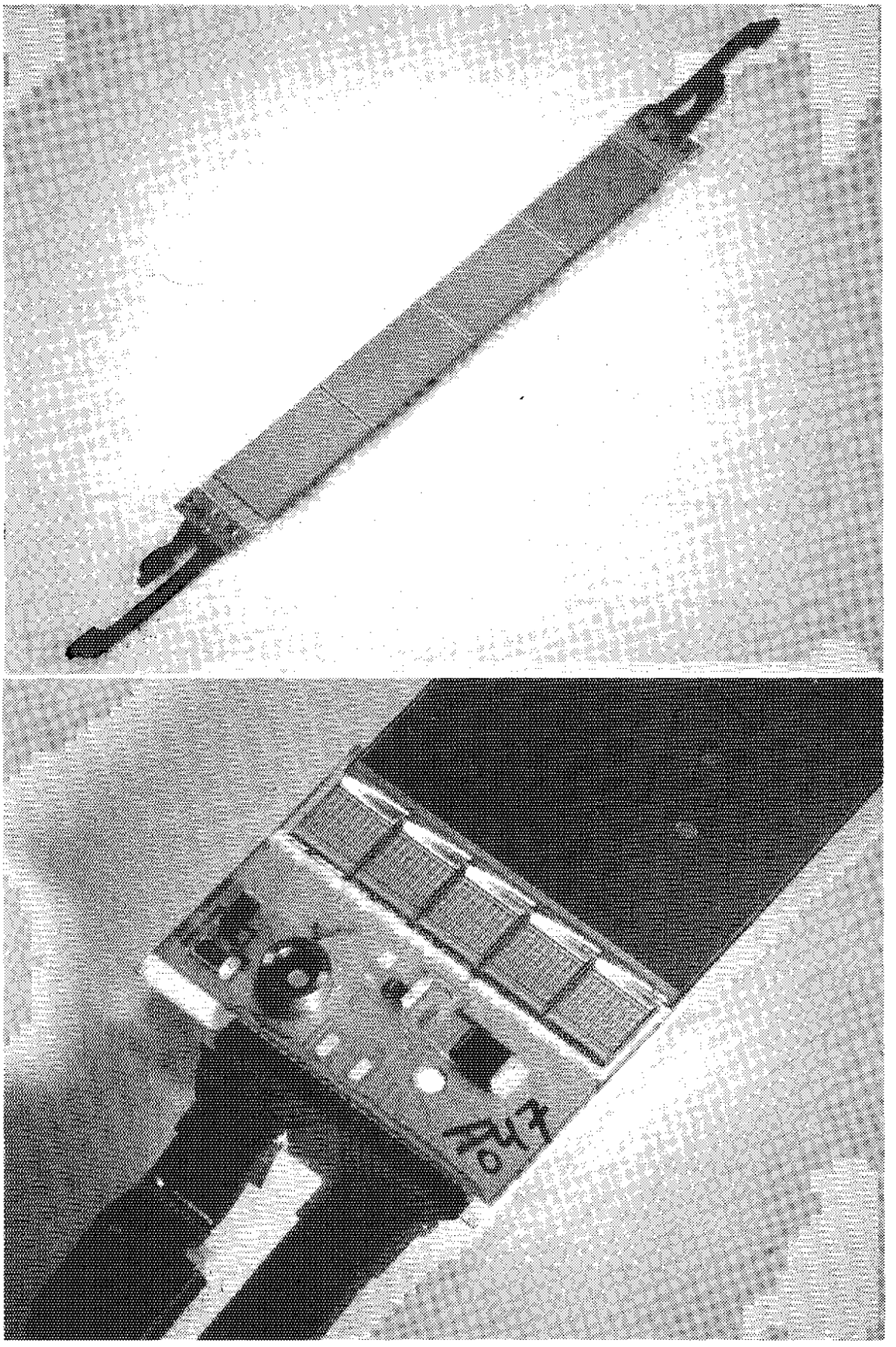

Figure 8: a) Outer layer detector module. b) Close-up of the readout hybrid.

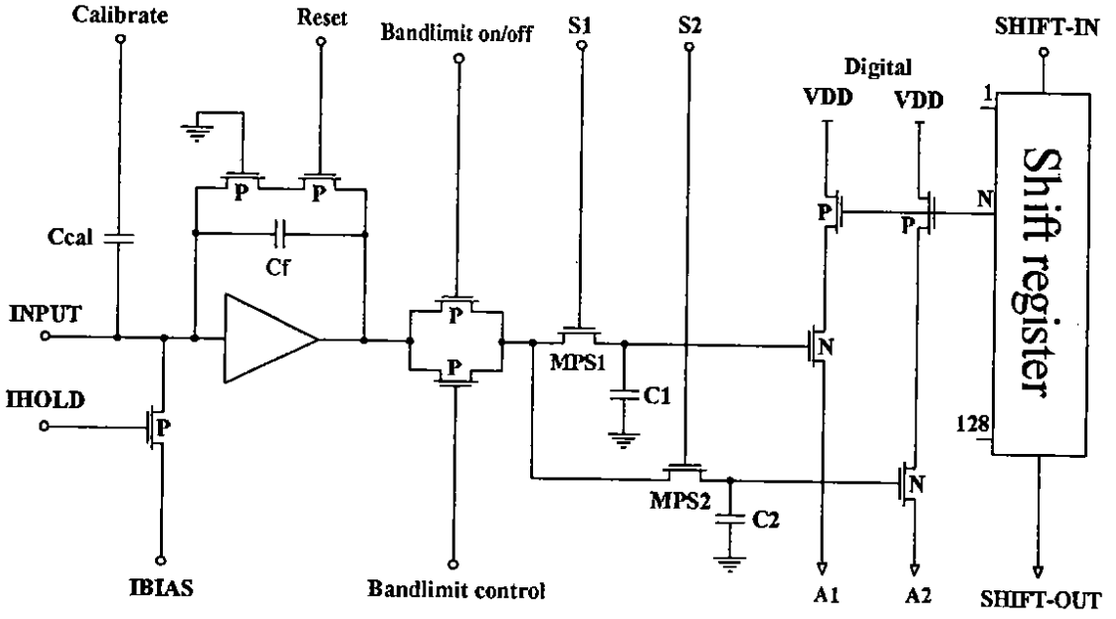

Figure 9: The MX3 integrated circuit. The 128 input pads are configured in two rows of 64 giving an effective pitch of 44 μm.

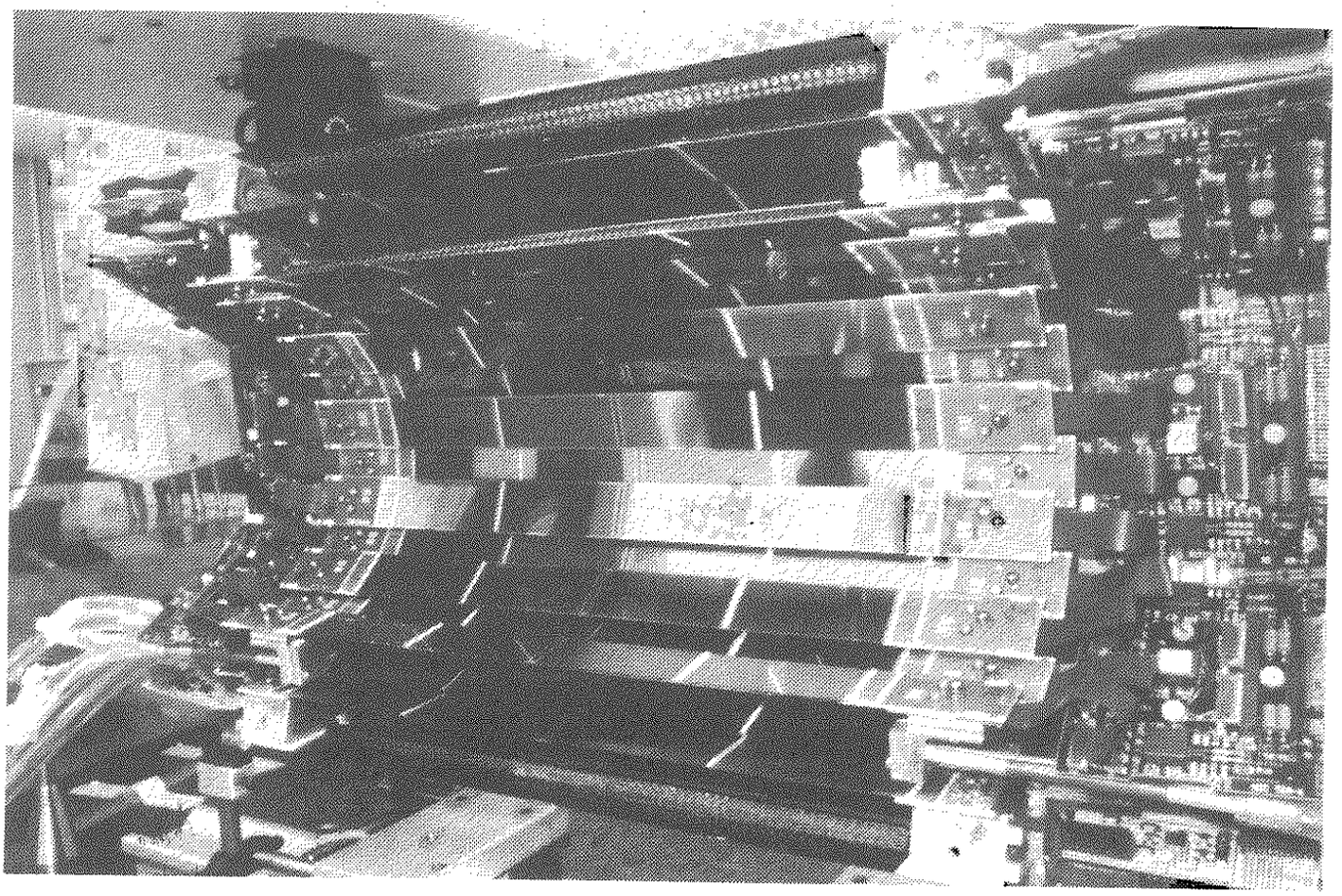

Figure 10: One half-shell with three silicon layers.

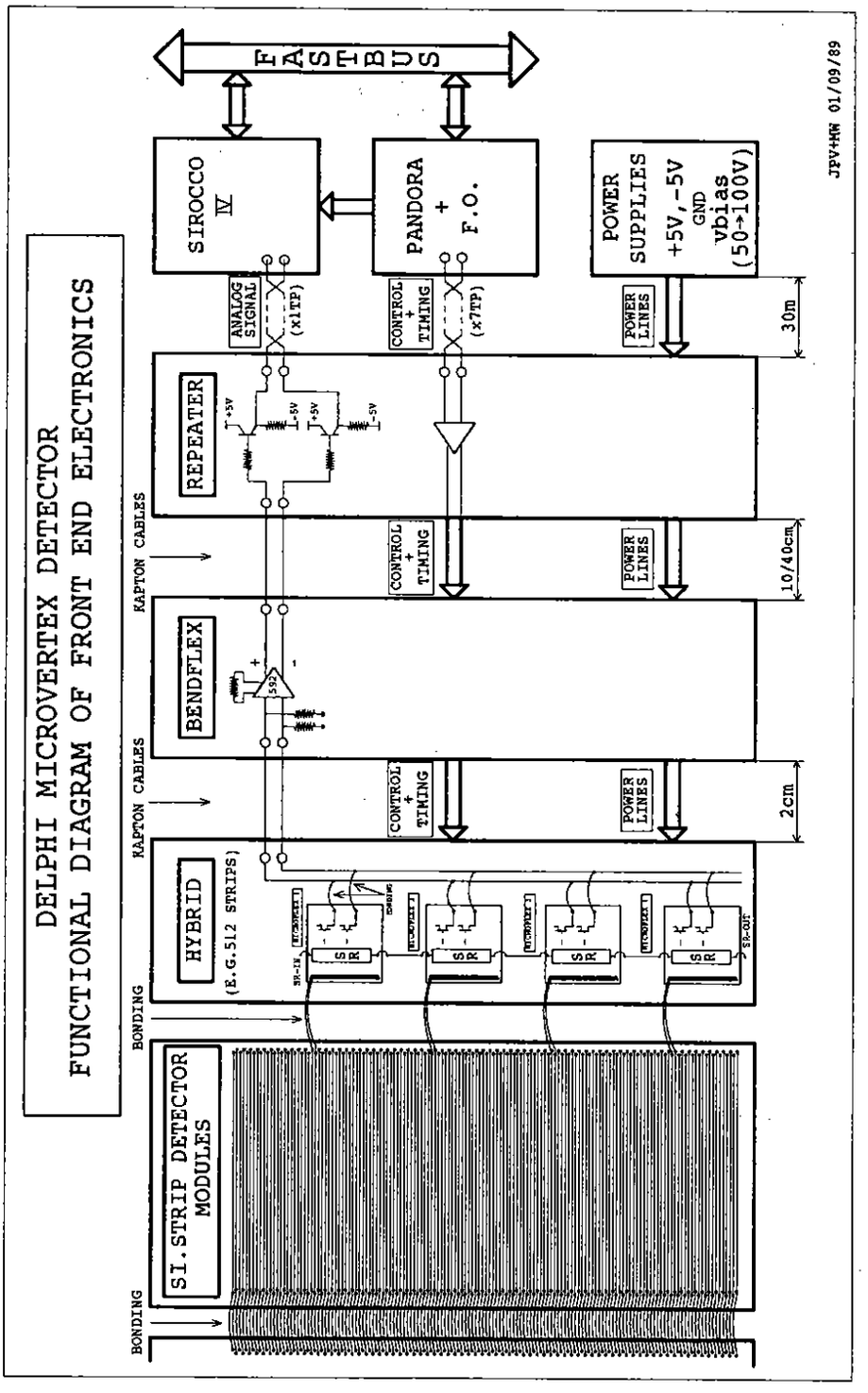

Figure 11: Functional diagram of the readout electronics.

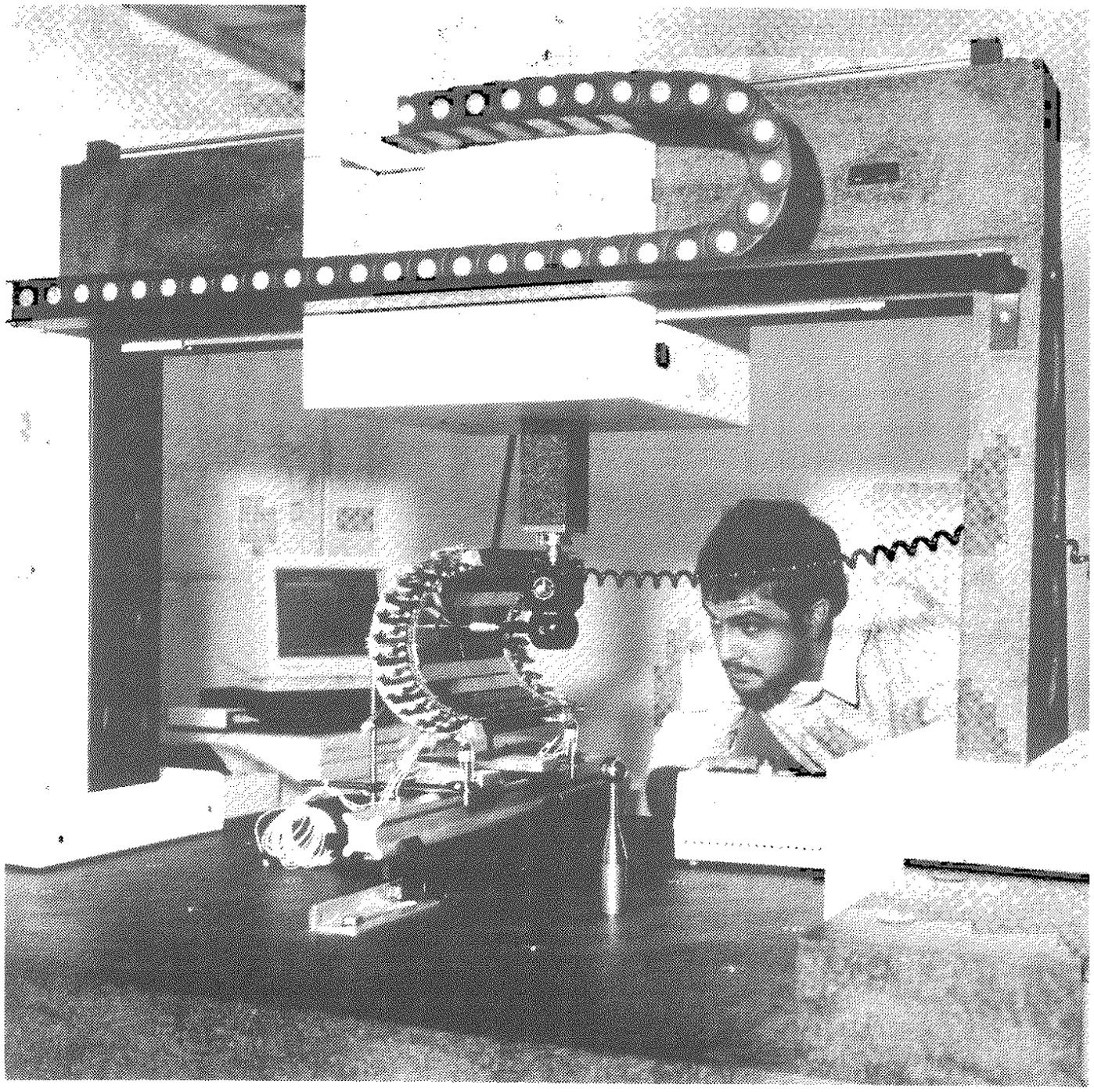

Figure 12: One half-shell during a survey session.

a

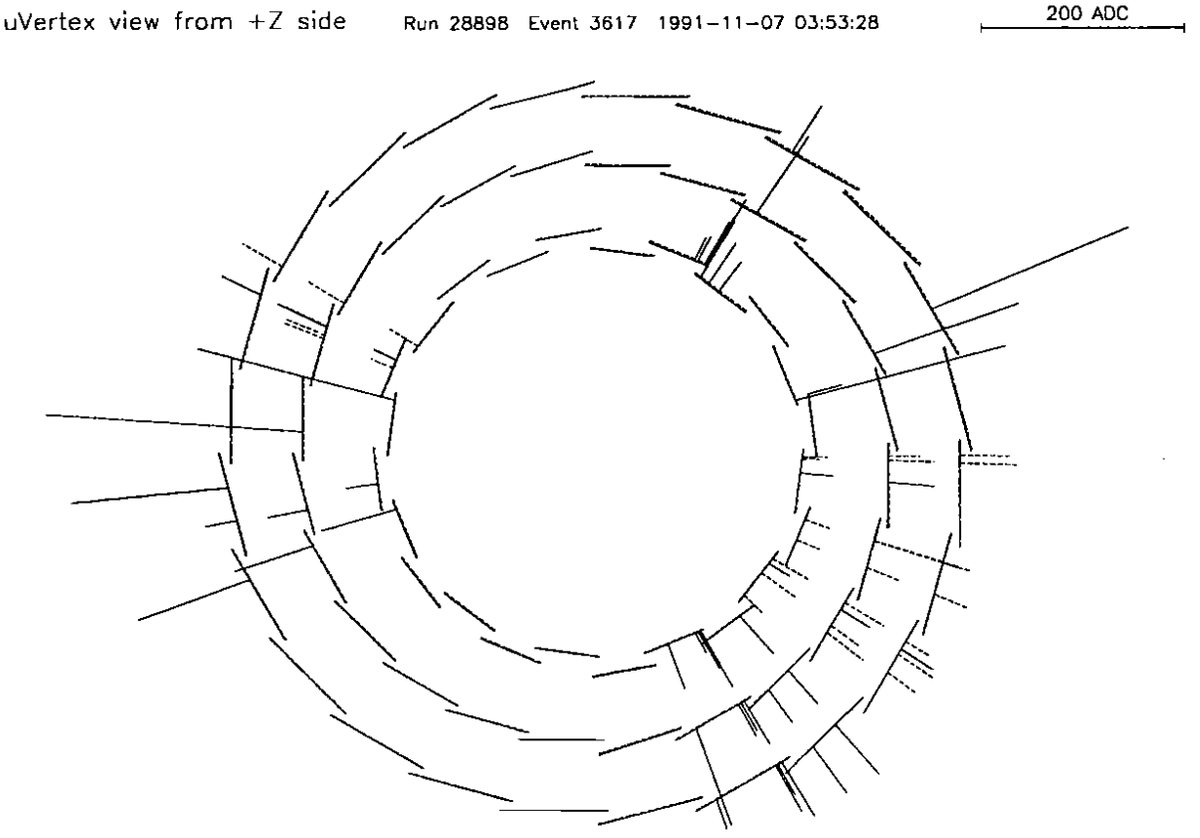

b

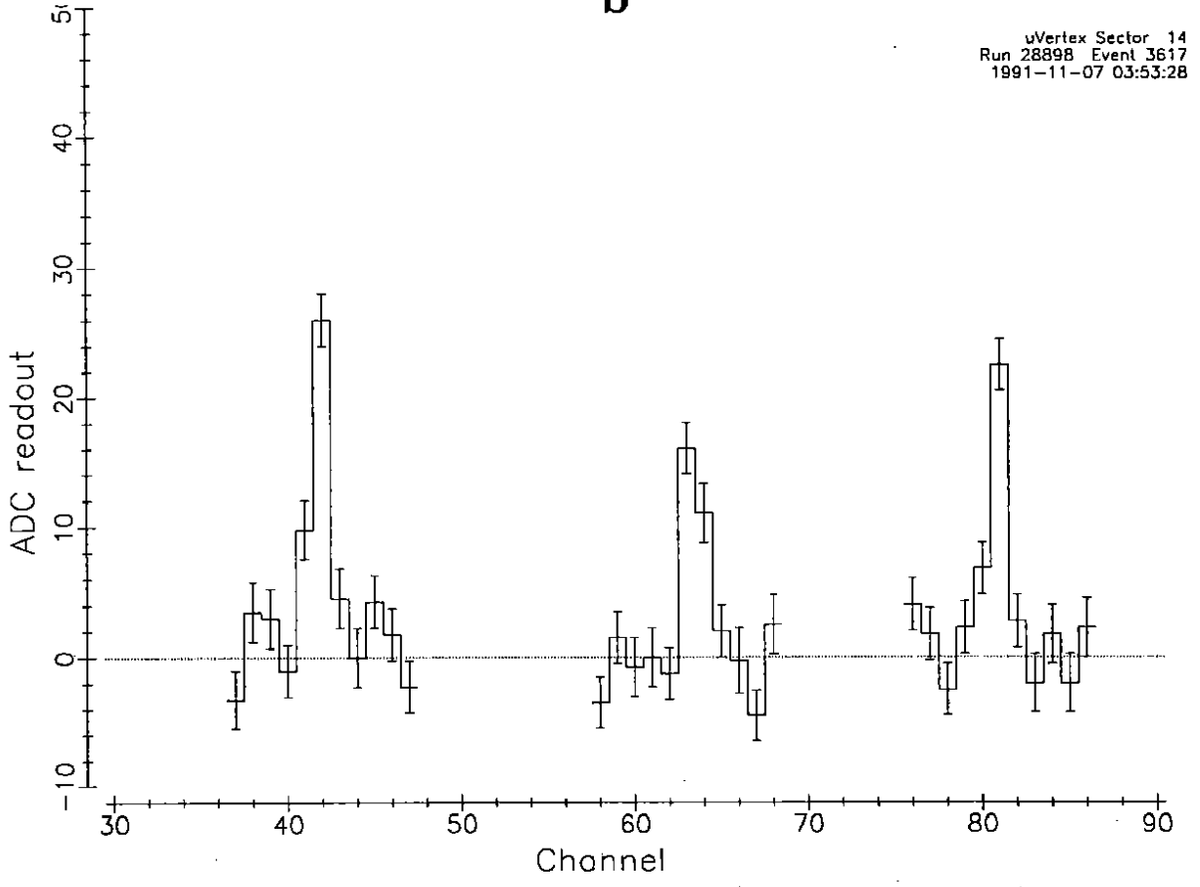

Figure 13: a)An on-line display of a hadronic Z^0 decay. b)A detail showing three adjacent clusters of this event.

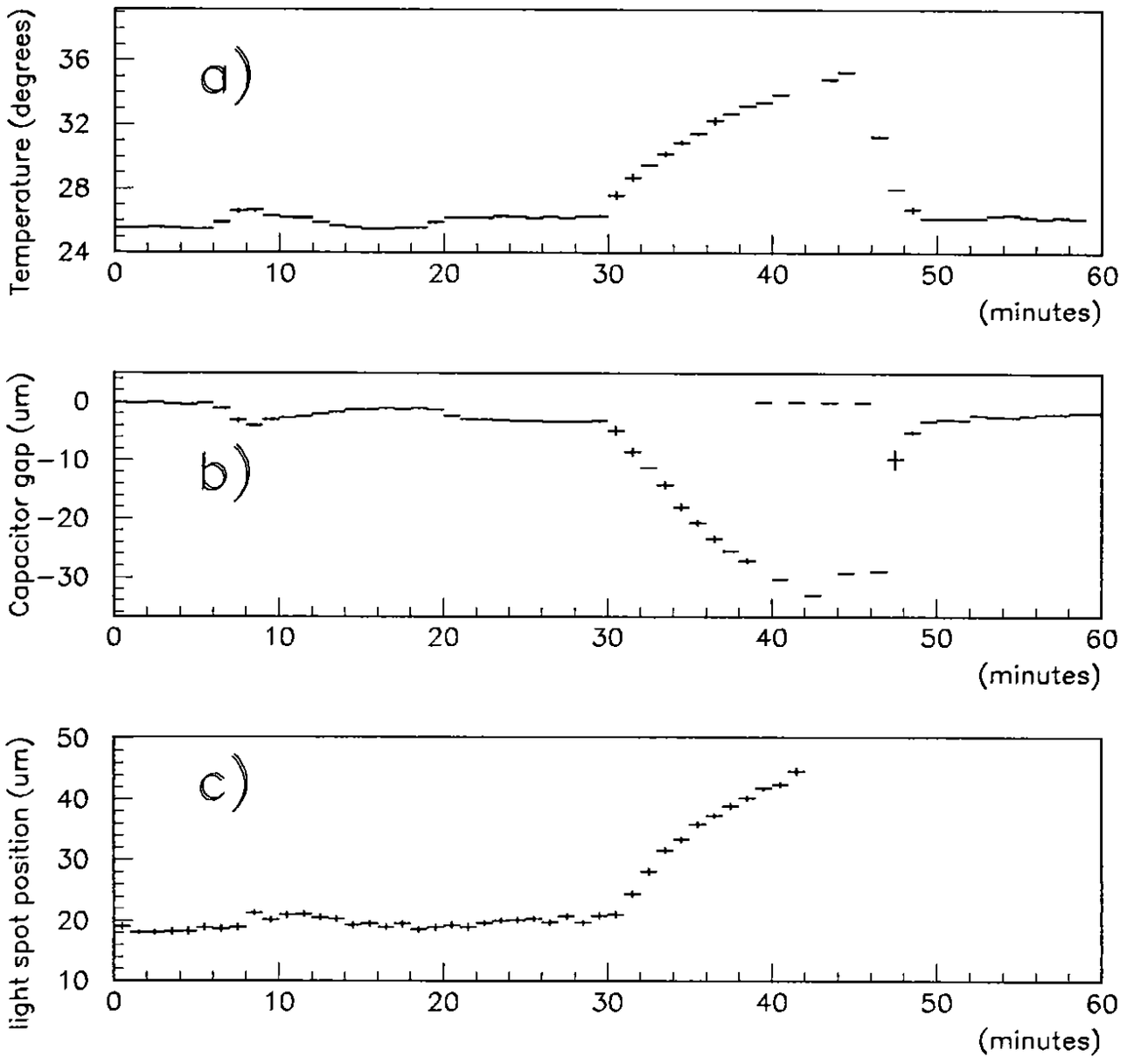

Figure 14: Response of the Microvertex Detector during a forced temperature scan: a) The detector support structure temperature. b) A radial gap as measured by the capacitive probes. c) A tangential light spot position.

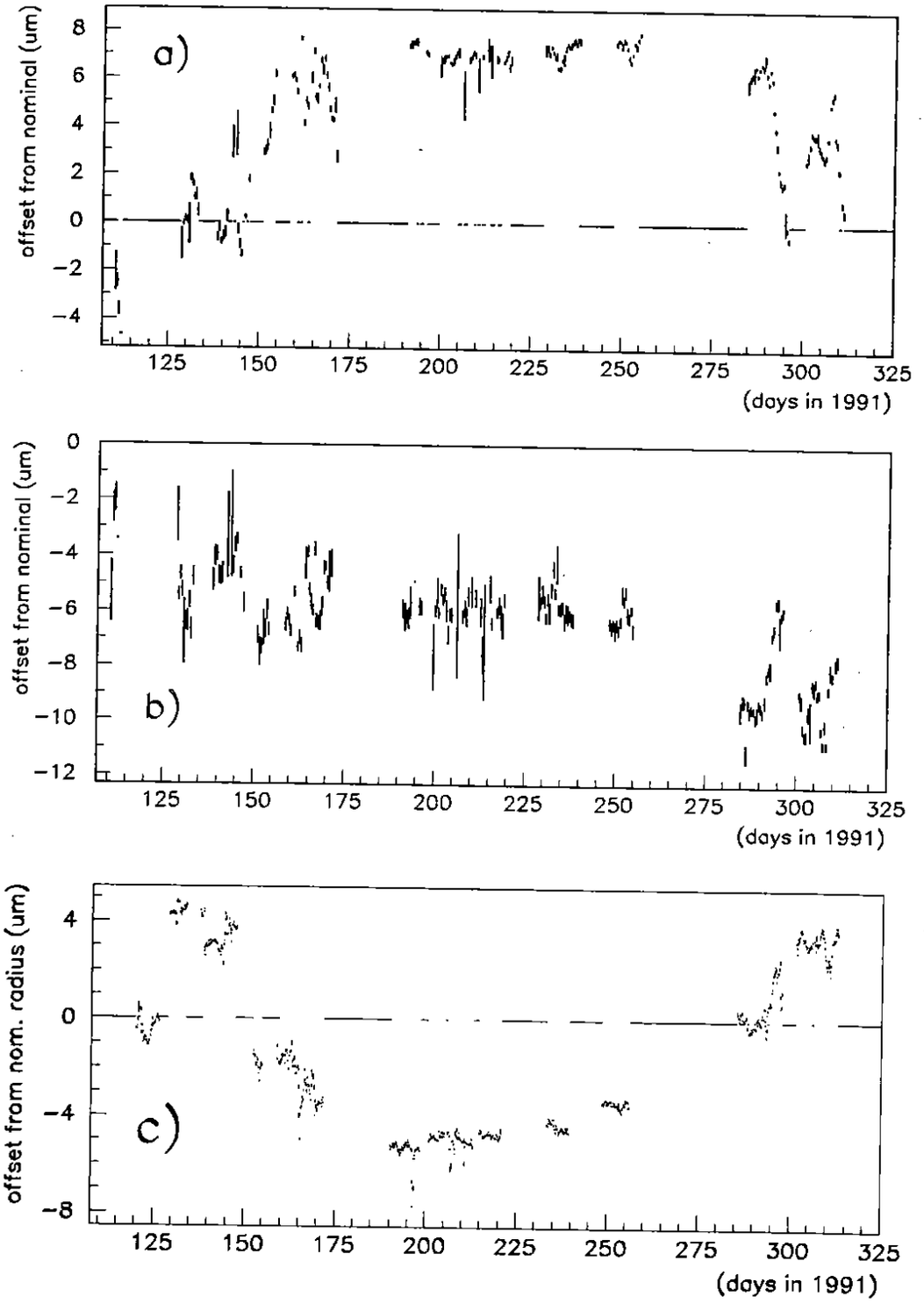

Figure 15: Light spot and capacitive probe position over the entire 1991 running period. a) A light spot on the top module in a half shell. b) A light spot on one from a bottom module in the half shell, which is more tightly constrained by the detector support structure. c) A radial position for the top capacitive probe.

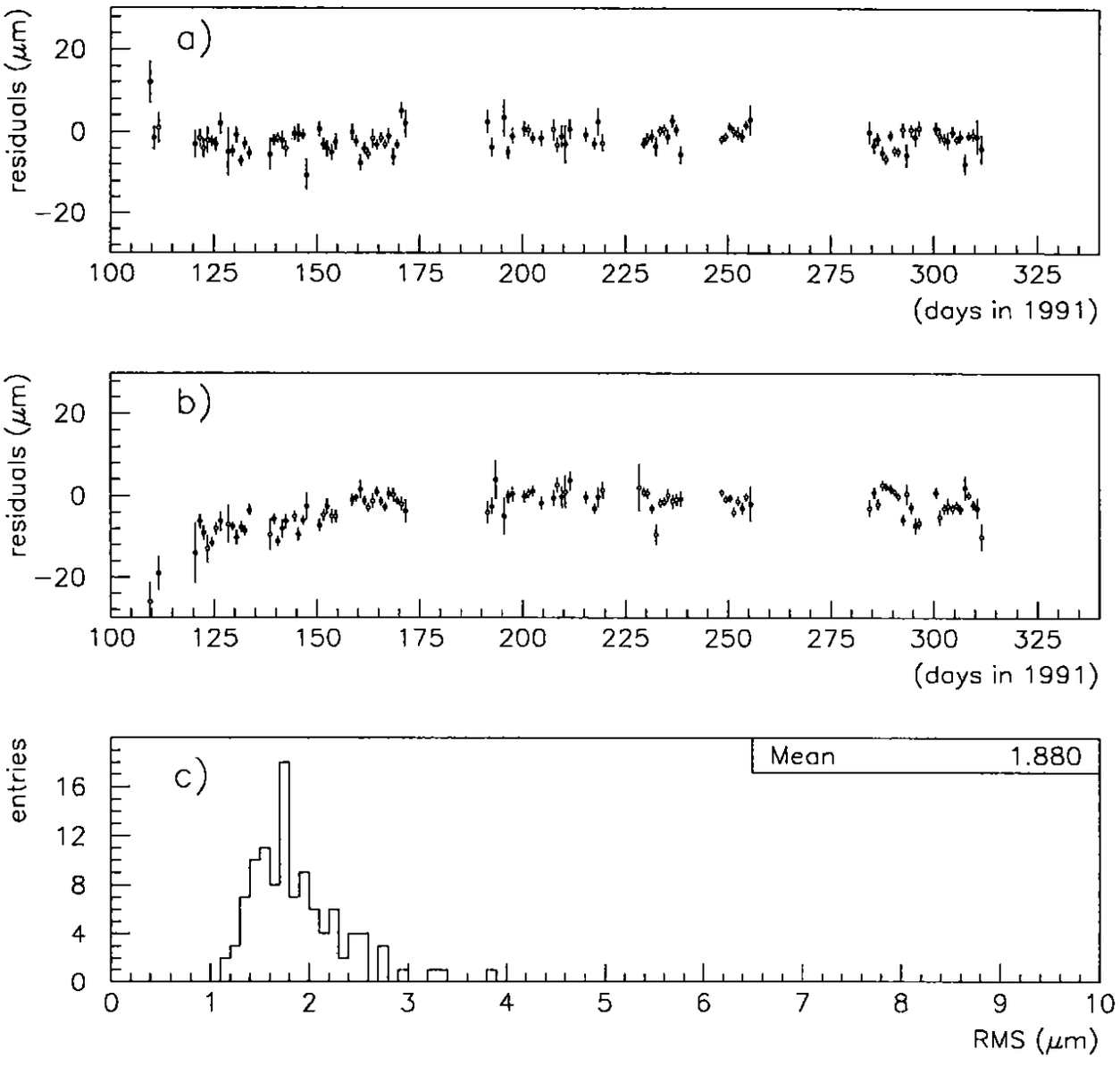

Figure 16: Sector overlap stability, measured with particle tracks. a) Residuals measured at the top half shell overlap. b) Residuals measured in an overlap within a half-shell. c) Histogram of RMS values of the 1991 residual distribution of all overlaps.

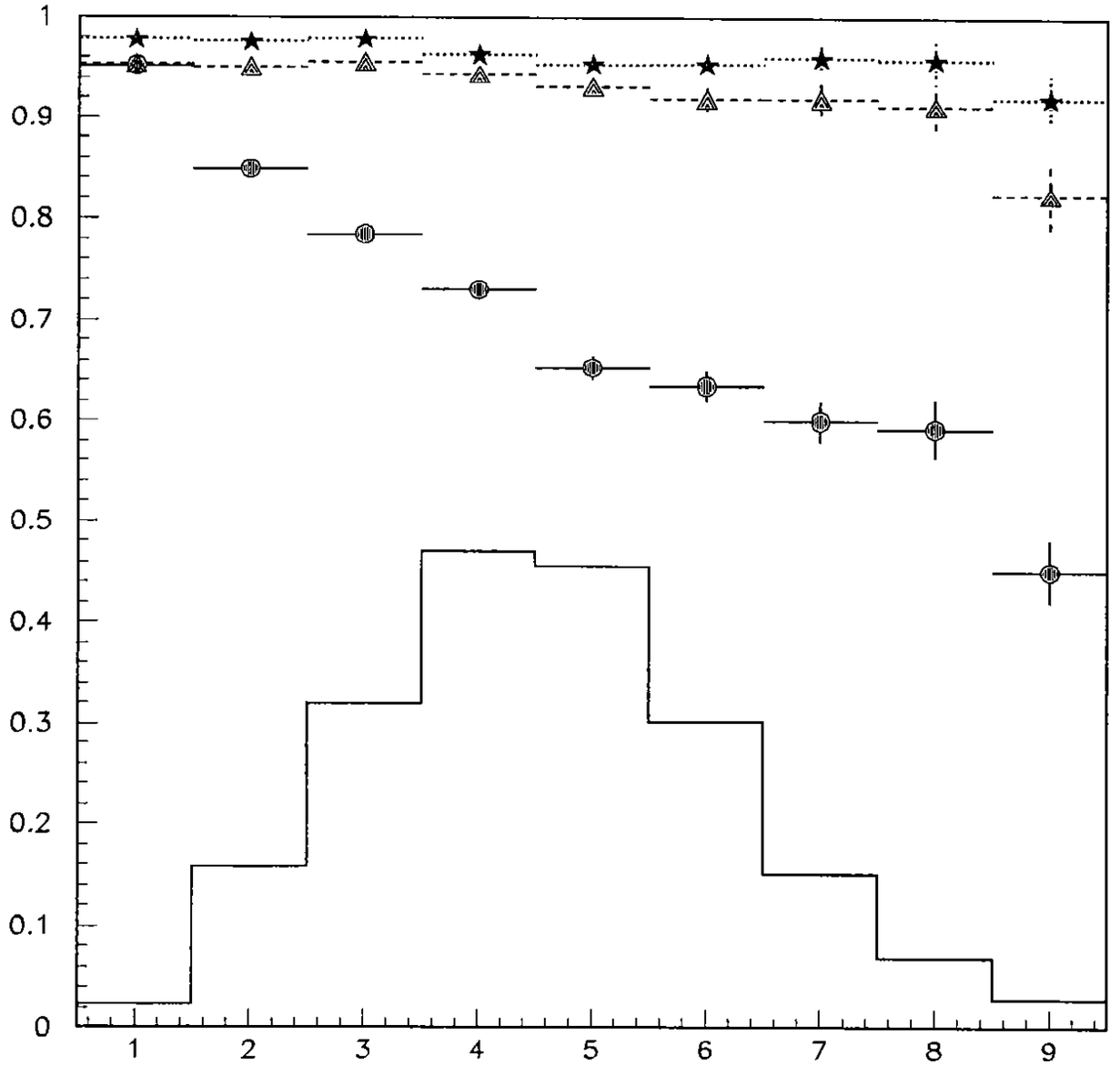

Figure 17: Fraction of tracks uniquely associated to clusters as a function of the local track multiplicity for the cases of one silicon layer (circles), two layers (triangles) and three layers (stars). The histogram shows the track multiplicity in the most hit sector for hadronic z^0 events.

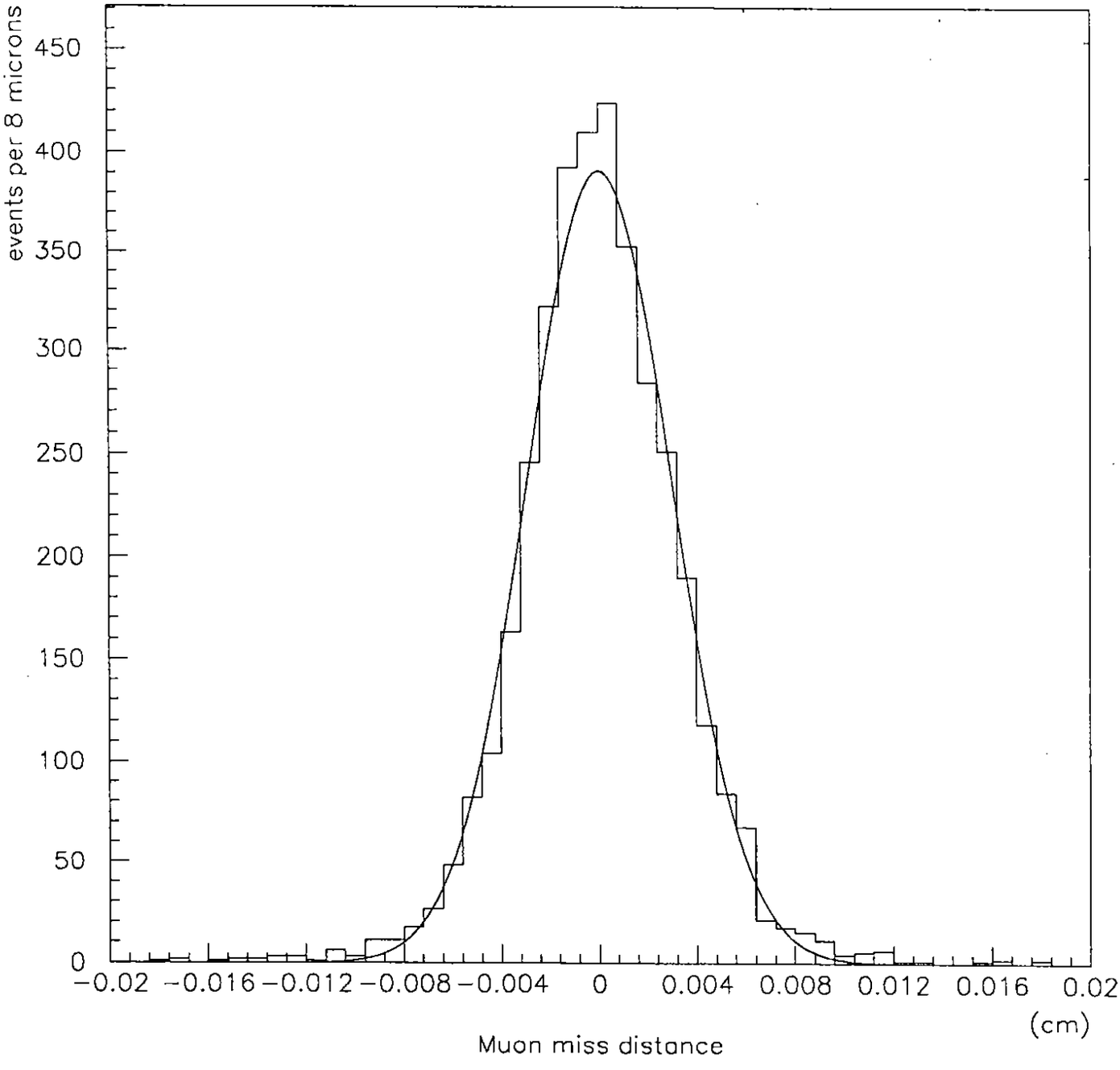

Figure 18: The distribution of the reconstructed distance between the two muons in $Z^0 \rightarrow \mu^+\mu-$ events.

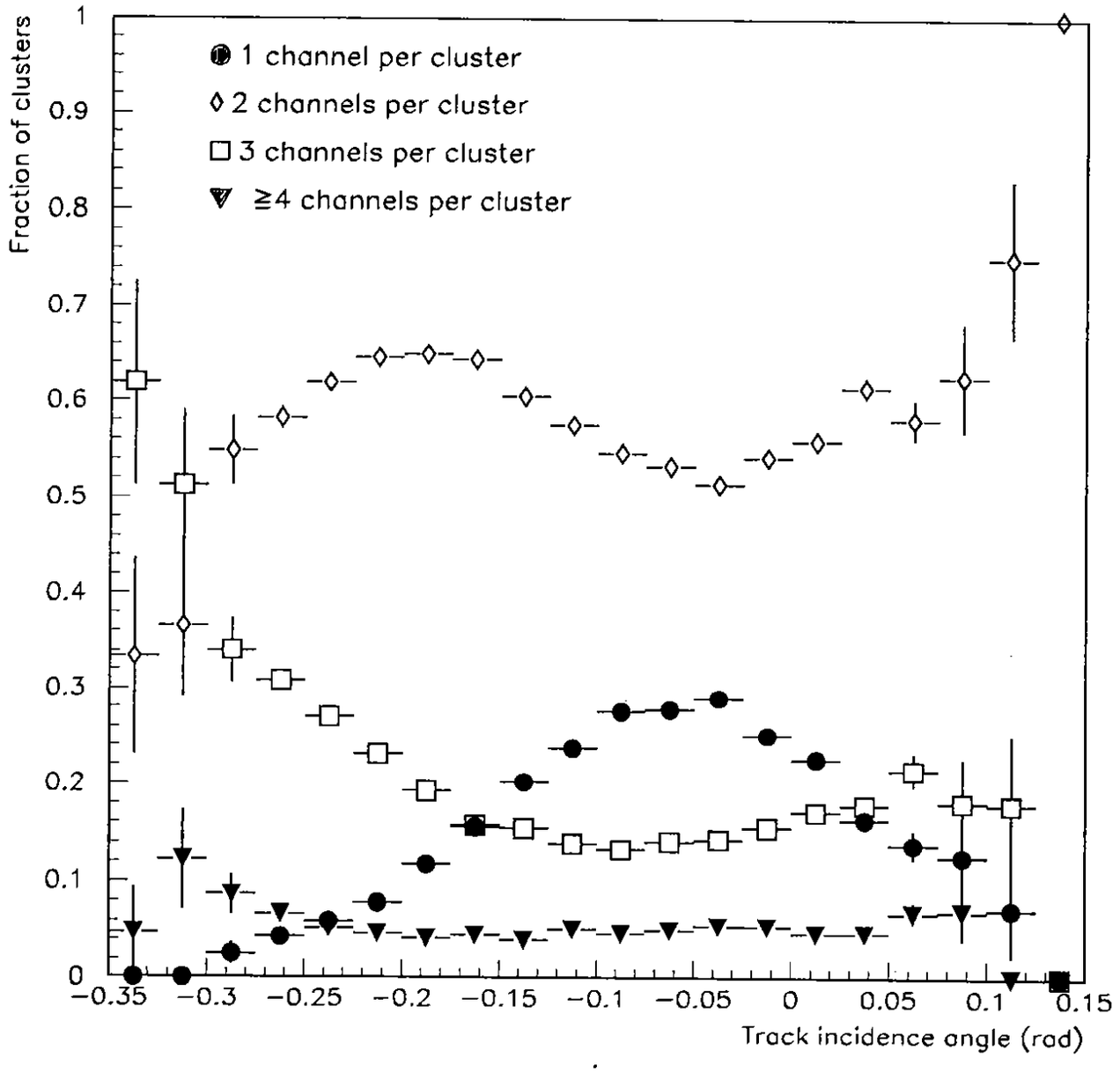

Figure 19: The fraction of clusters with 1, 2, 3 and more than 3 channels per cluster as a function of the incidence angle of a track in the silicon.

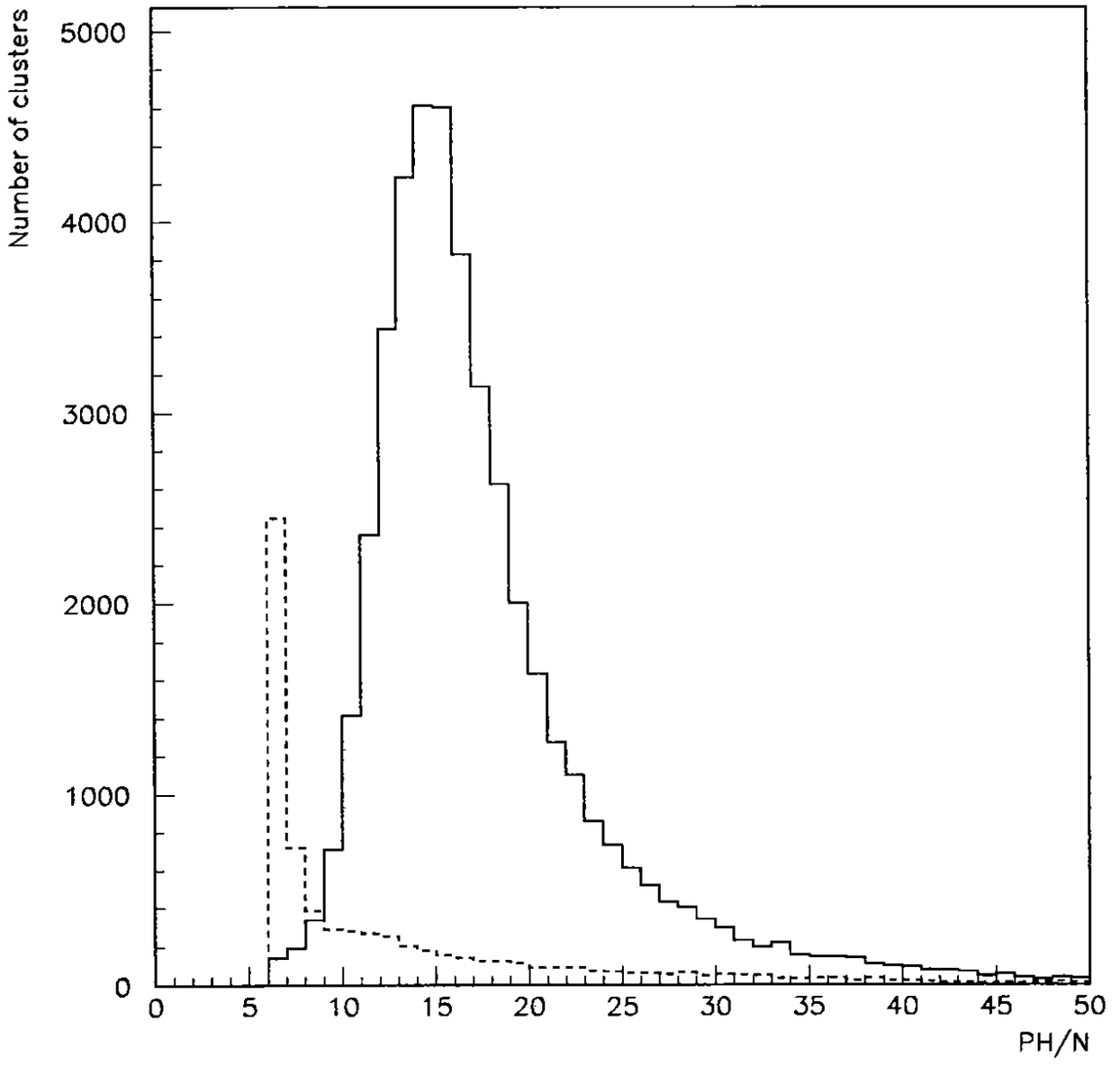

Figure 20: PH/N for clusters with (full-line) and without (dashed-line) a track associated to them for the Inner layer modules. The PH/N has been normalized to the minimum track length in traversing the silicon.

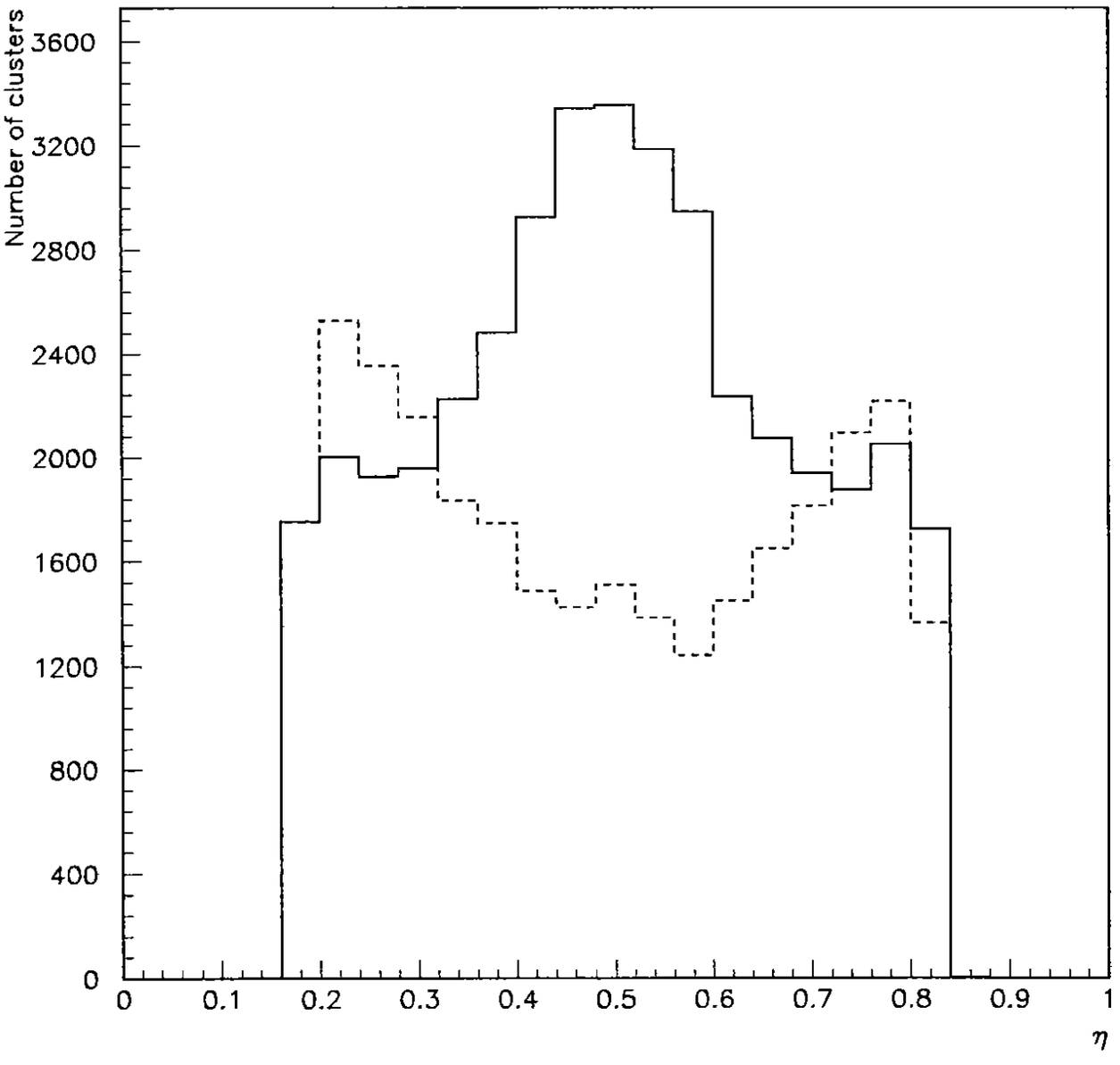

Figure 21: The η distribution for tracks traversing the silicon with an angle relative to the Lorentz angle of 0.15-0.25 rad (full-line) and < 0.05 rad (dashed-line). Note that due to the definition of η (see text), η is restricted to $0.17 < \eta < 0.83$, all remaining clusters contain only one channel by definition and are not included in these distributions.

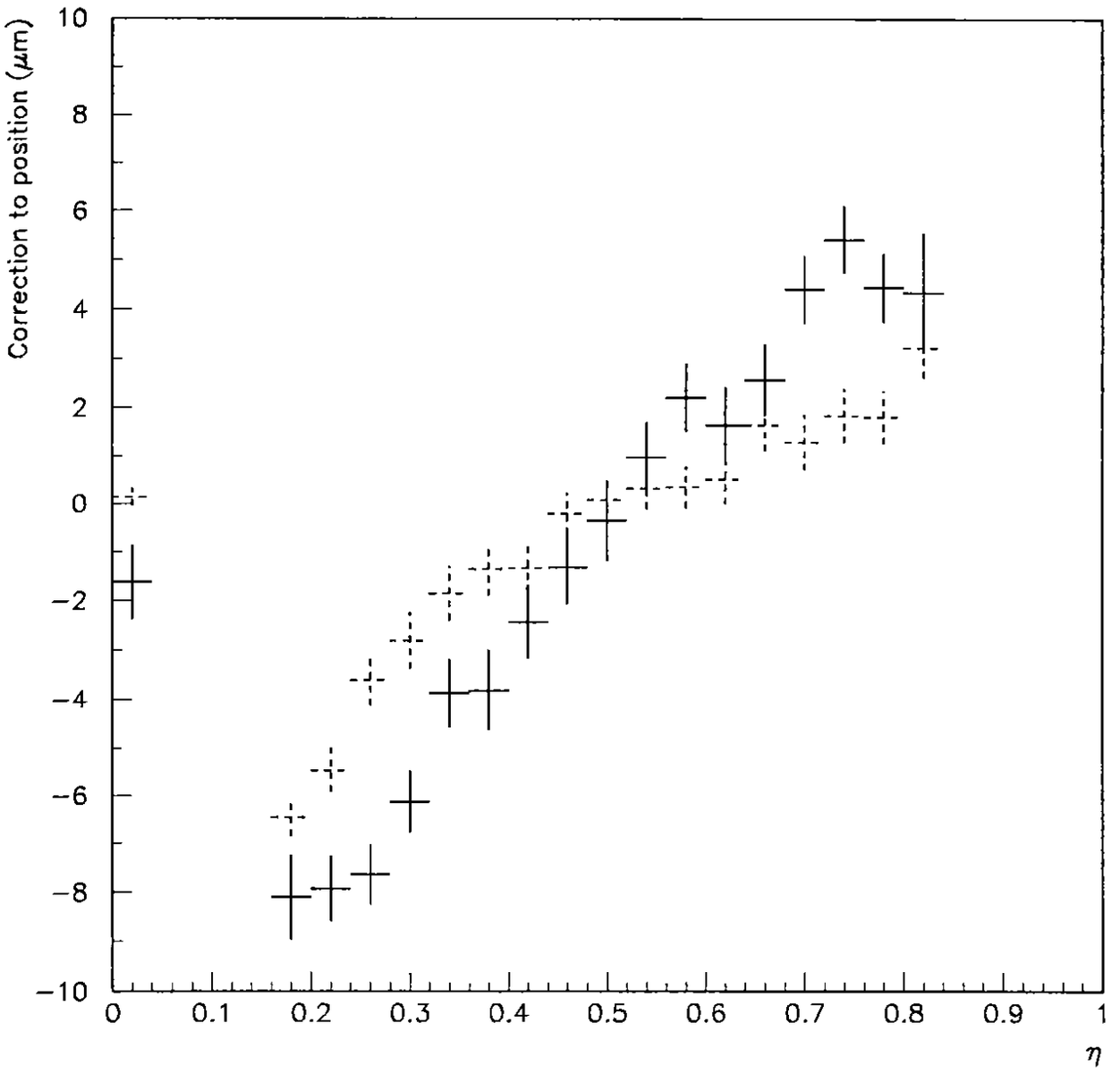

Figure 22: Difference between hit position in the Inner layer and a track defined by Closer and Outer layers as a function of η for tracks traversing the silicon at large (full-line) and small (dashed-line) angles. Note that due to the definition of η (see text), η is restricted to $0.17 < \eta < 0.83$. All remaining clusters contain only one channel by definition and are included in these distributions at η=0.

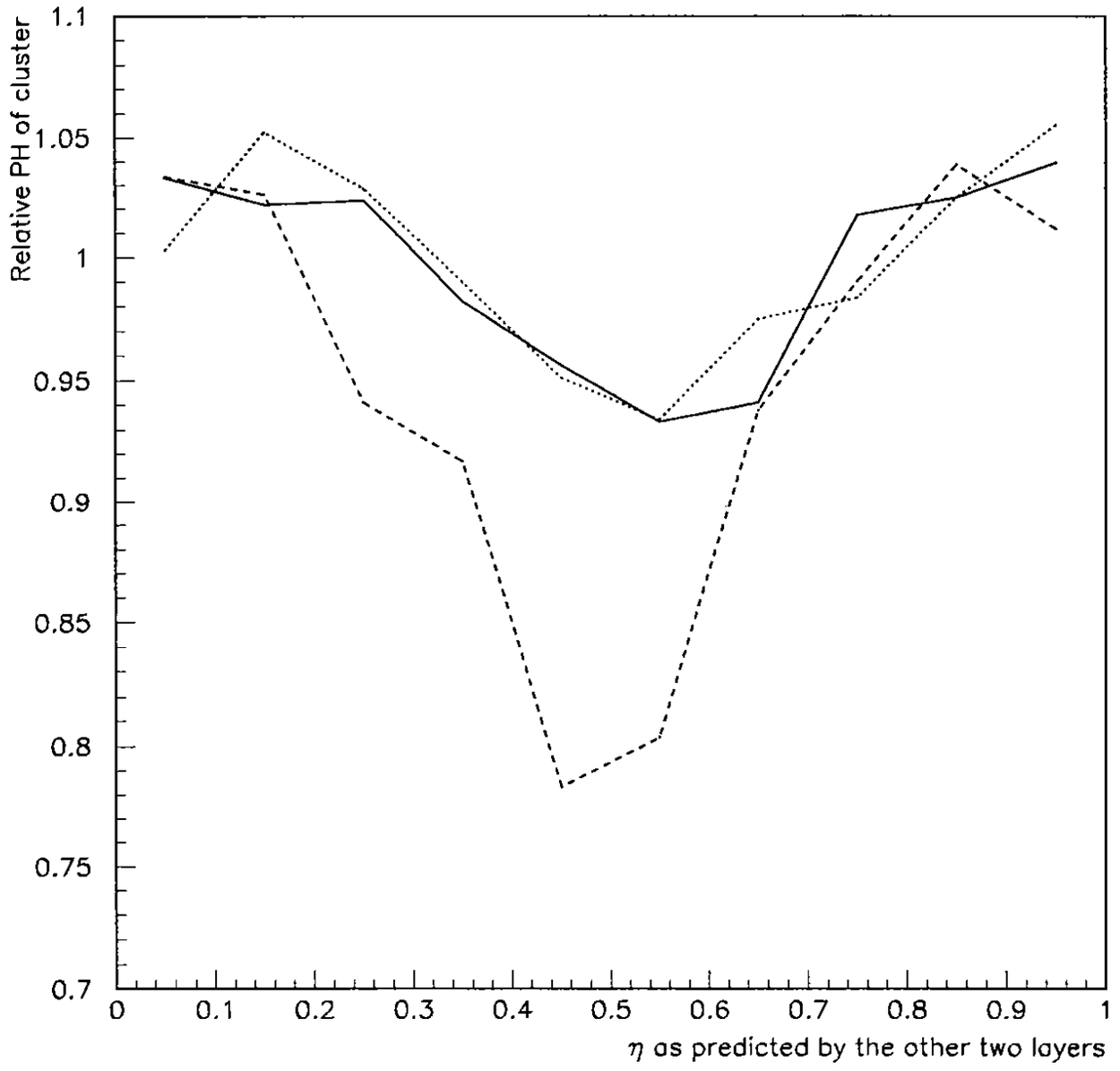

Figure 23: Relative PH of a cluster as a function of η for Closer (full-line), Inner (dashed-line) and Outer (dotted-line) layers.

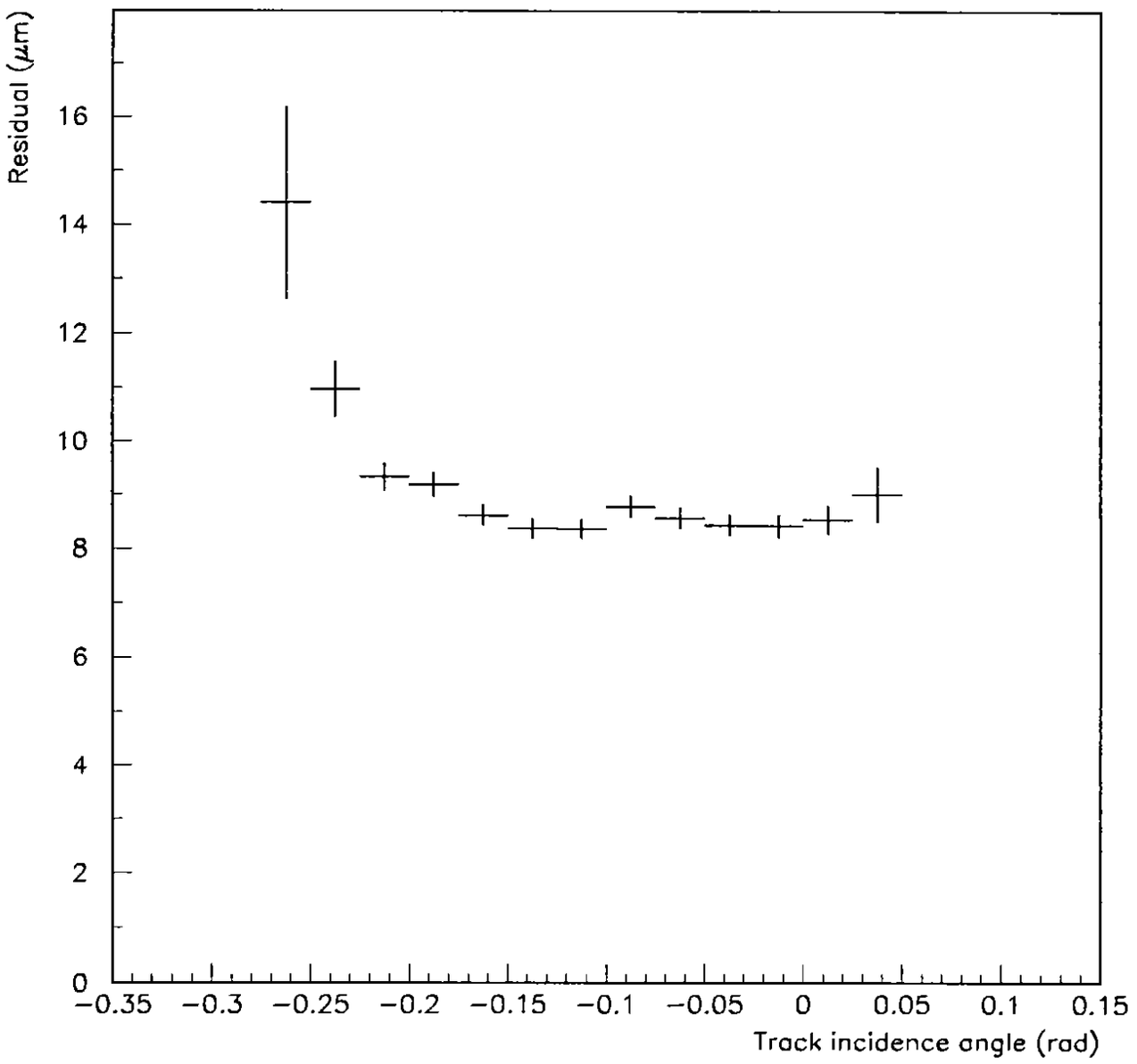

Figure 24: The residual of a hit in the Inner layer relative to a track as defined by the Closer and Outer layers as a function of the incidence angle of a track for all clusters, using only the 2 largest PH in a cluster to determine η. To convert the residual to a hit precision multiply by 0.82 (see text).

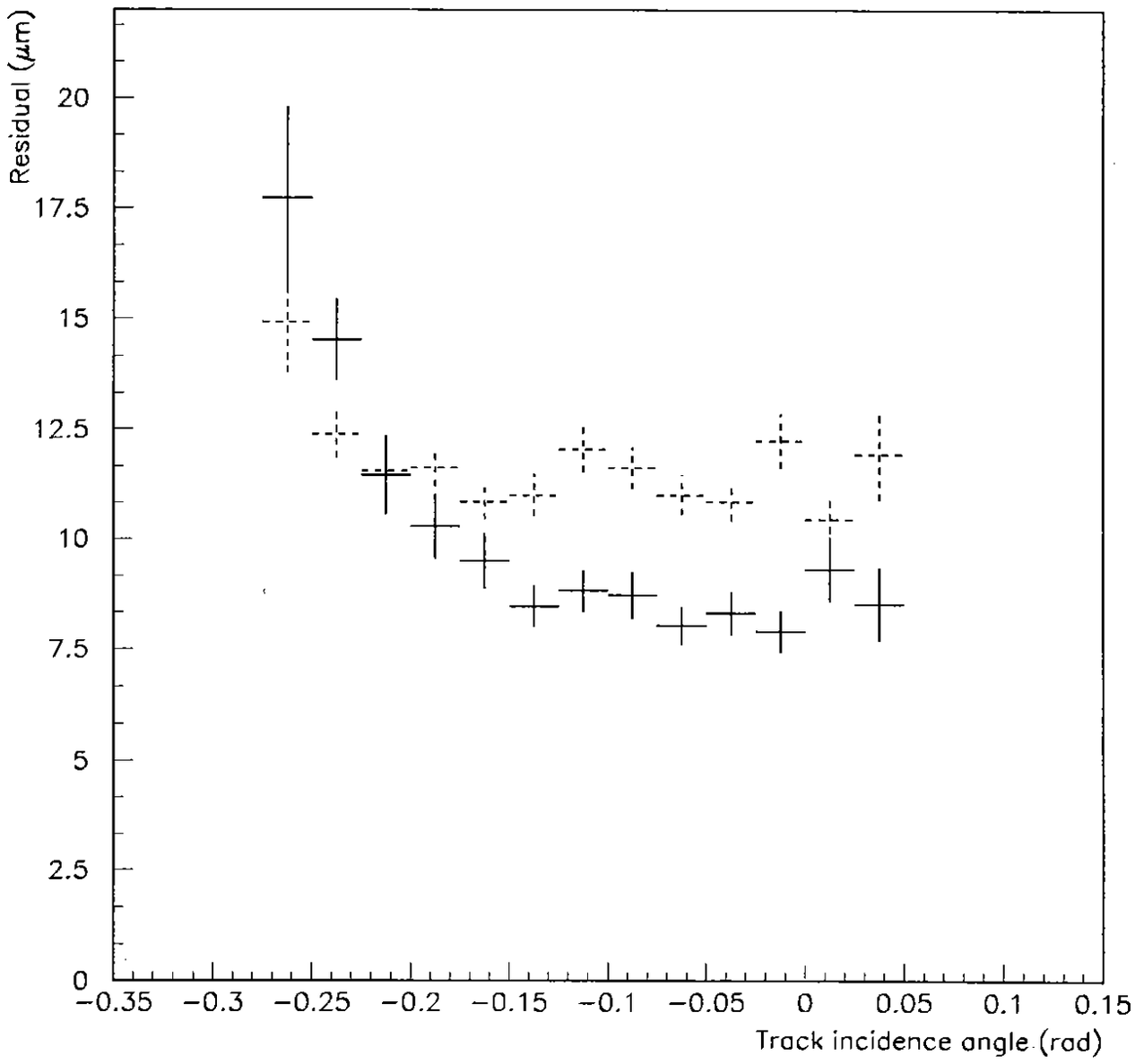

Figure 25: The residual of a hit in the Inner layer relative to a track as defined by the Closer and Outer layers as a function of the incidence angle of a track. To convert the residual to a hit precision multiply by 0.82 (see text). Only clusters with 3 channels are included. The full and dashed lines refer to the two η algorithms as described in the text.

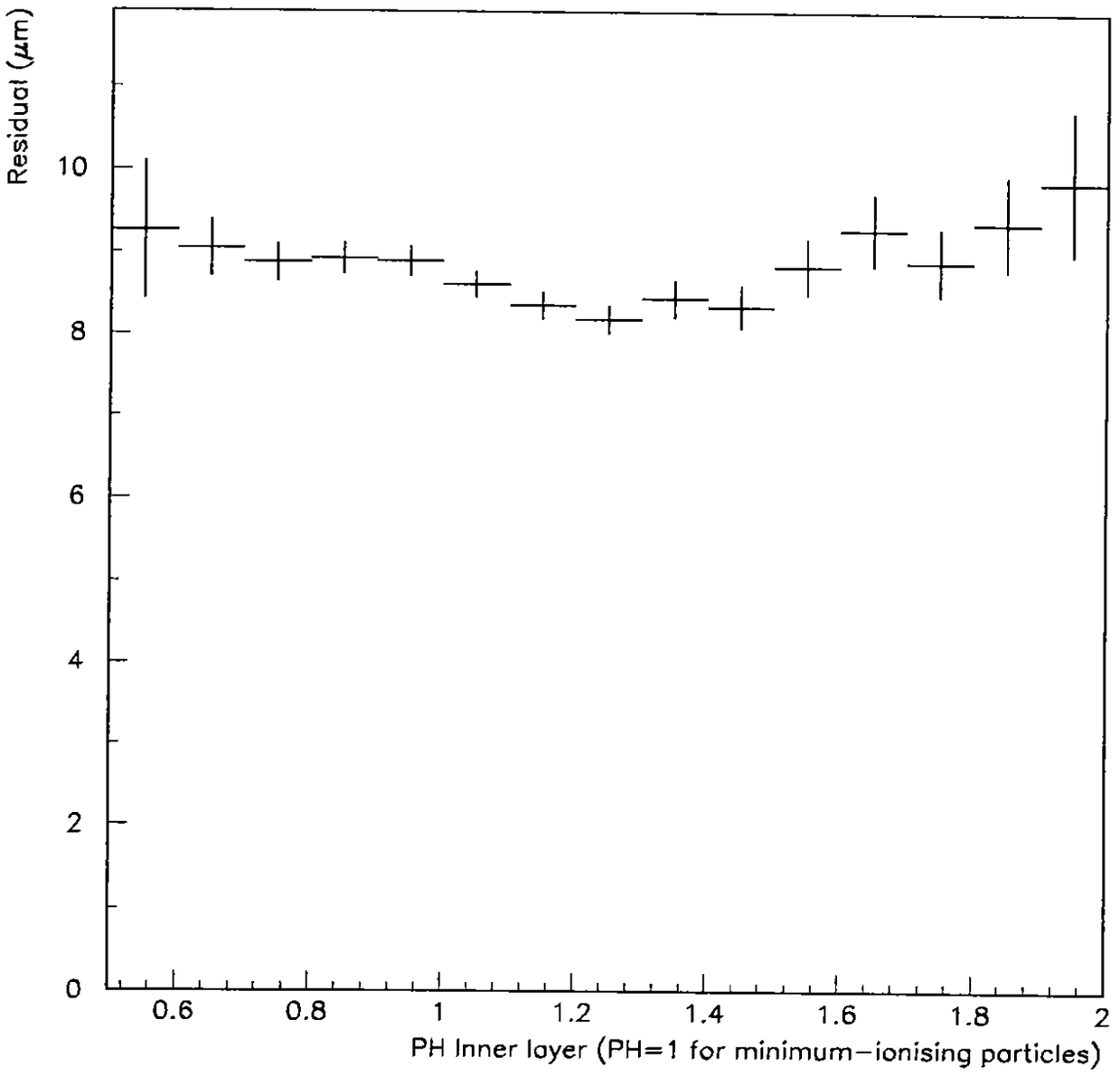

Figure 26: The residual of a hit in the Inner layer relative to a track as defined by the Closer and Outer layers as a function of the PH of a cluster in the Inner layer. To convert the residual to a hit precision multiply by 0.82 (see text).

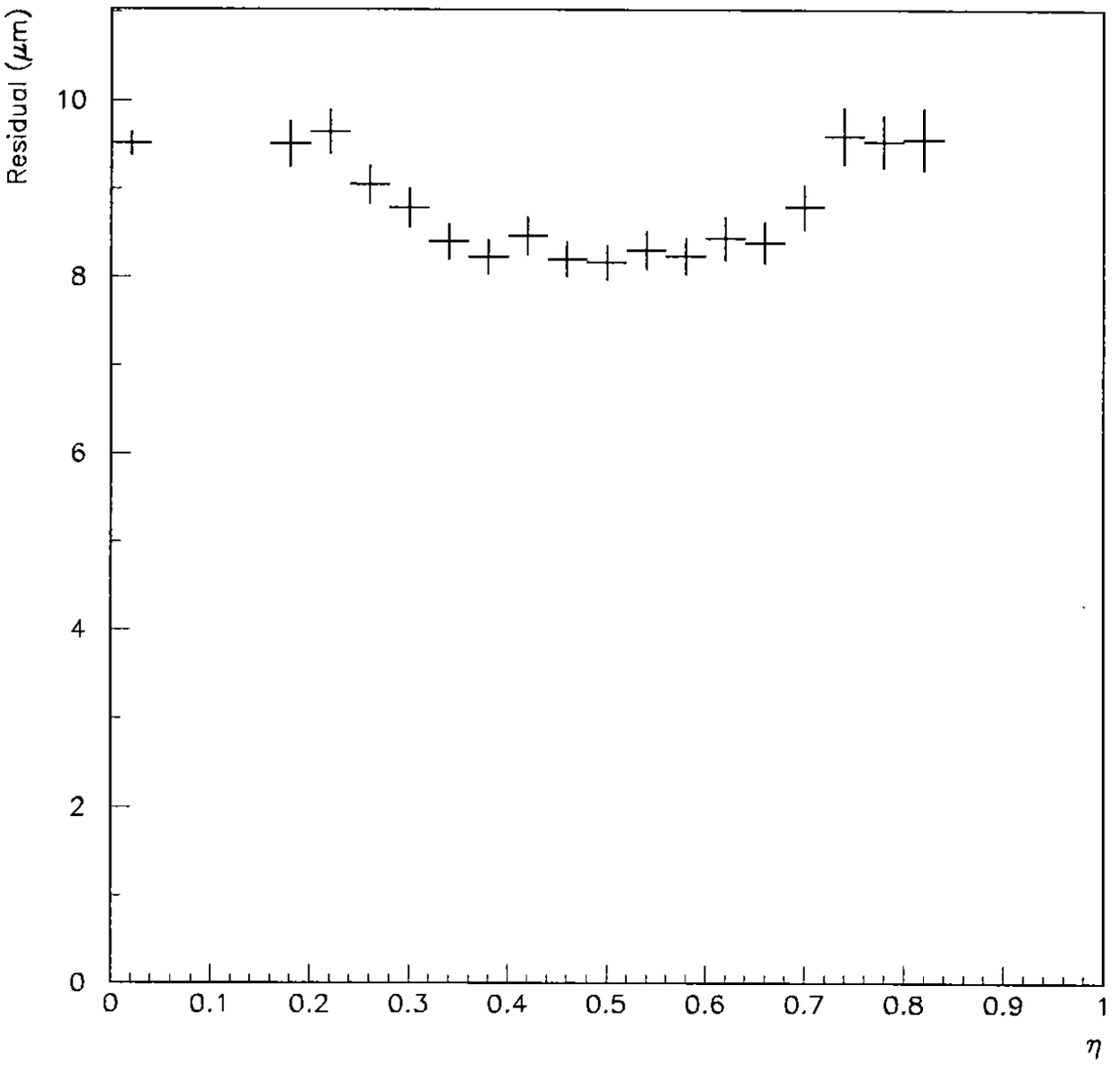

Figure 27: The residual of a hit in the Inner layer relative to a track as defined by the Closer and Outer layers as a function of η. To convert the residual to a hit precision multiply by 0.82 (see text). Note that due to the definition of η (see text), η is restricted to $0.17 < \eta < 0.83$. All remaining clusters contain only one channel by definition and are included in this distribution at η=0.

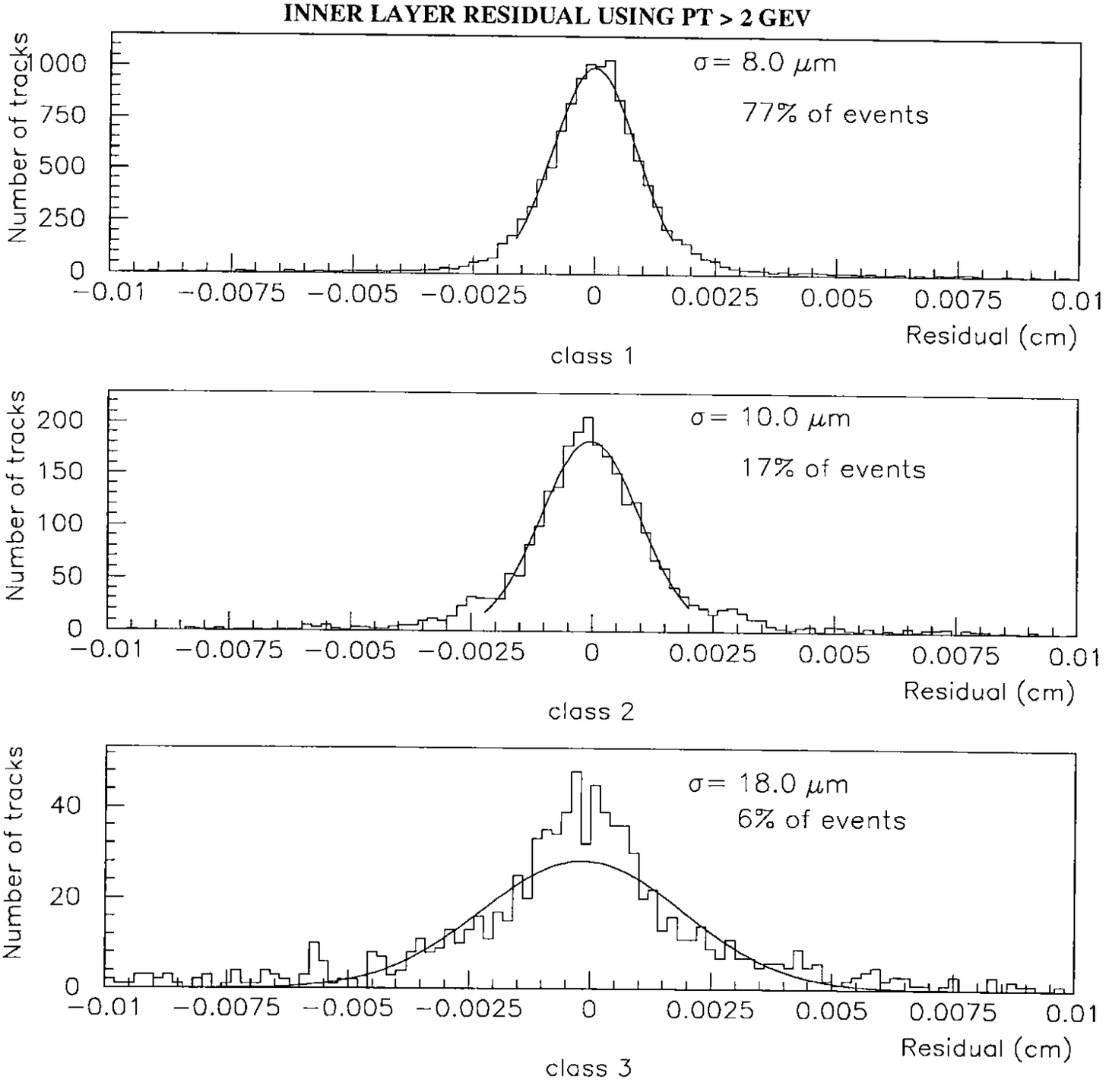

Figure 28: The residual of a hit in the Inner layer relative to a track as defined by the Closer and Outer layers as a function of the three categories of cluster types, which are defined in the text. To convert the residual to a hit precision multiply by 0.82 (see text).

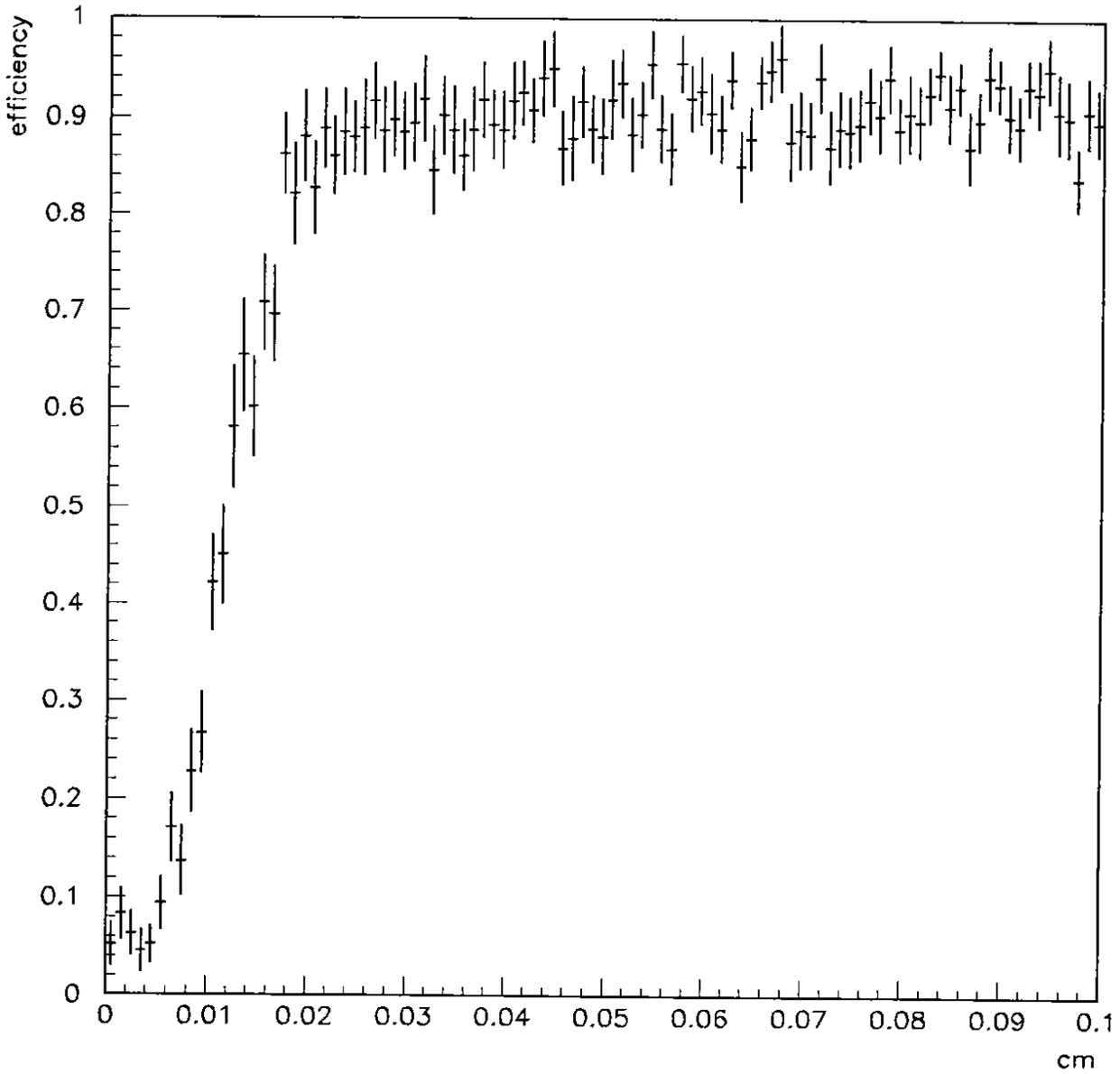

Figure 29: Efficiency for two tracks to be associated to clusters in a silicon layer as a function of the track separation.

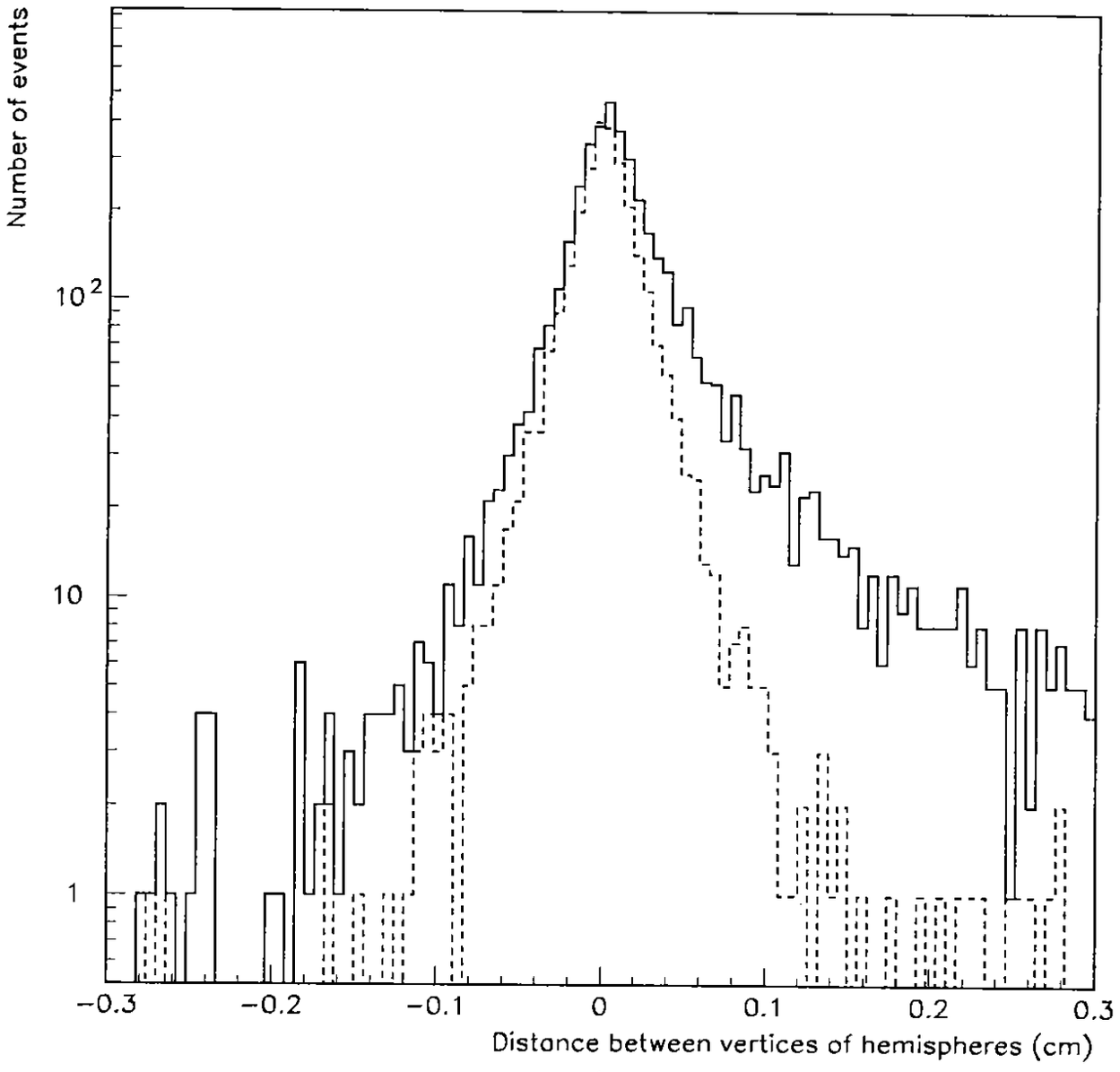

Figure 30: The longitudinal distance between two vertices constructed in the two hemispheres of the events. The full-line is for vertices with a χ^2 probability less than 10%, the dashed-line for the other events.

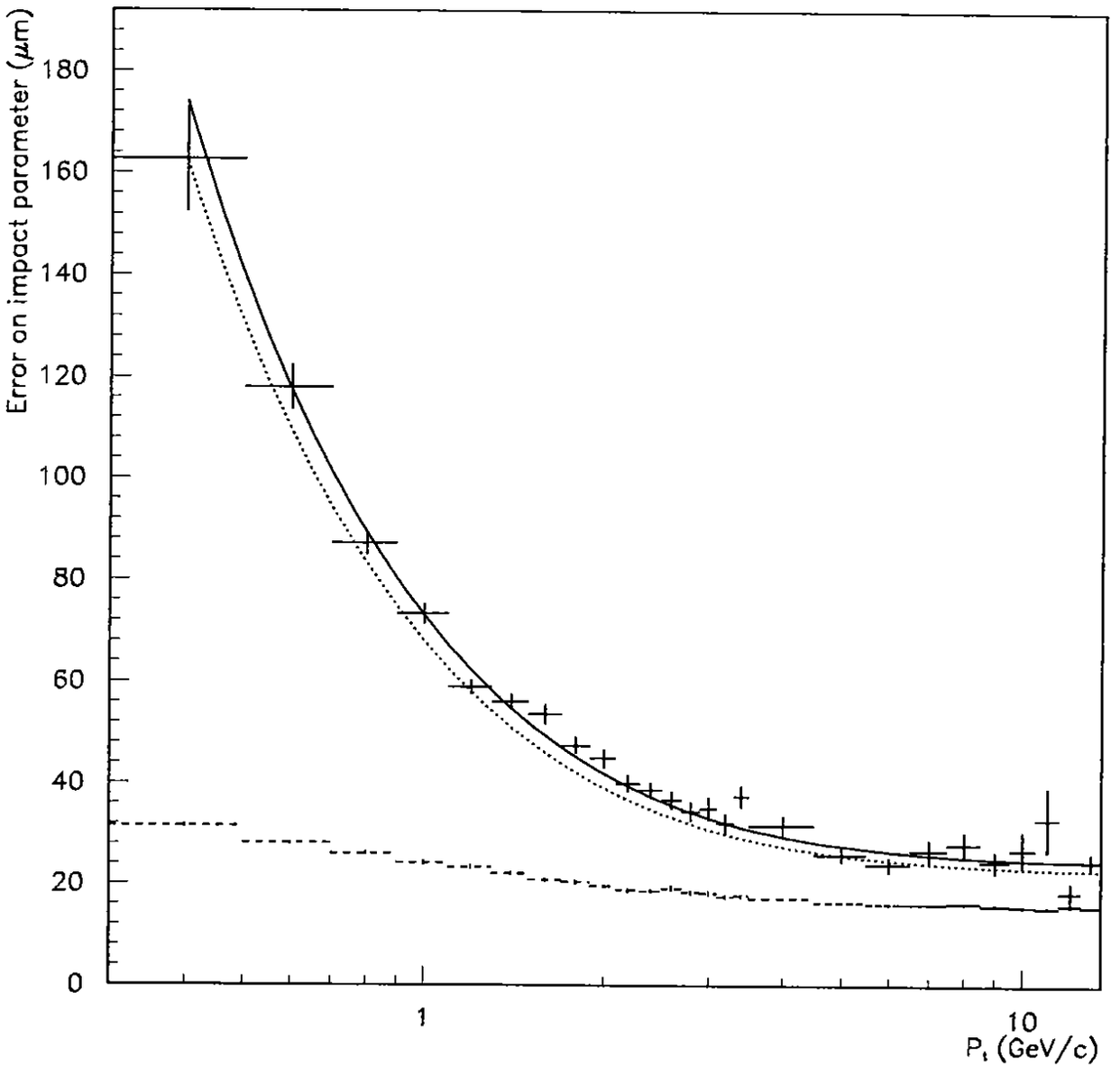

Figure 31: The error on the impact parameter as measured as a function of p_t in real data. The dashed data gives the contribution from the error on the vertex, which has been subtracted quadratically from the error per track. The full line is a fit to $\sqrt{69^2/p_t^2 + 24^2}\mu$m ($p_t$ in GeV/c). The expected error transverse to tracks at the beamspot is represented with a dotted line.